Air-Brayton Cycle Concentrated Solar Power future plants via redox oxides-based structured thermochemical heat exchangers / thermal boosters

Deliverable D4.3.

Structured objects geometries and design of dual-bed unit for integrated TCS/thermal booster operation

Dissemination Level: Public

WP4: Dual-bed prototype design and solar thermal power plant level system integration scenarios

Date: 30.06.2025

https://www.abraytcspfuture.eu/

This project has received funding from the European Union's Horizon Europe research and innovation programme under grant agreement no 101084569.

Disclaimer

The work described in this document has been conducted within the ABraytCSPfuture project that is co-funded by the European Union. Views and opinions expressed herein are however those of the author(s) only and do not necessarily reflect those of the European Union or of the granting authority, European Climate, Infrastructure and Environment Executive Agency (CINEA). Neither the European Union nor the granting authority can be held responsible for them.

Grant Agreement Number: 101084569	**Acronym: ABraytCSPfuture**			
Full Title	**A**ir-**Brayt**on Cycle **C**oncentrated **S**olar **P**ower **future** plants via redox oxides-based structured thermochemical heat exchangers/thermal boosters			
Call Topic Identifier:	HORIZON-CL5-2021-D3-03			
Funding Scheme	HORIZON EUROPE, RIA – Research and Innovation Actions			
Project start date:	01.11.2022			
Project duration:	48 months			
Project URL	https://www.abraytcspfuture.eu/			
EU Project Officer	Clara Astudillo Llorente			
Project Coordinator	DLR – German Aerospace Center			
Deliverable	DD4.3. Structured objects geometries and design of dual-bed unit for integrated TCS/thermal booster operation			
Date of Delivery	Contractual	30.10.2024	Actual	30.06.2025
Nature	Report			
Dissemination Level	Public			
Lead Beneficiary	TEKNIKER			

Document History

Version	**Issue Date**	**Change History**	**Authors**	**Organisation**
1.0	27.06.2025	Document drafted	Ignacio, Guisasola Saioa, Herrero López	TEKN
1.1	28.06.2025	Updated with final partner feedback	C. Agrafiotis G. Karagiannakis	DLR CERTH
1.2	29.06.2025	Final review	G. Karagiannakis	CERTH
1.3	30.06.2025	Suggested changes implemented	S. Herrero	TEKN

About the Project

ABraytCSPfuture (ABCSPF) sets forth an innovative, carbon-neutral way for implementing the highly efficient air-Brayton gas turbine power generation cycles into future air-operated Concentrated Solar Power (CSP) plants. Air-Brayton cycles are used in traditional power plants where, however, involve fossil fuels combustion via pressurized air. *ABraytCSPfuture*'s carbon-neutral approach aims at achieving higher solar-to-electricity efficiencies, vital for competitiveness of CSP and non-reachable by either PVs or molten salts and thermal oils, increasing in parallel significantly the plants' storage capability. The project will develop and demonstrate a first-of-its-kind compact, dual-bed thermochemical reactor/heat exchanger unit that will transfer heat from a non-pressurised air stream to a pressurised one, while also operating as a thermal booster, raising the temperature of the pressurized stream to the level required for Brayton cycles. Furthermore, the volumetric solar energy storage density of air-operated CSP plants will be significantly increased by rendering their current sensible-only regenerative storage systems to hybrid sensible-thermochemical storage ones within the same storage volume. Both these functionalities will be materialized by thermochemical reactor/heat exchanger units comprised of non-moving, flow-through porous ceramic structures (honeycombs or foams) based on earth-abundant, cost-efficient, non-toxic oxide materials and exploiting reversible reduction/oxidation reactions of such oxides in direct contact with air, accompanied by significant endothermic/exothermic heat effects. The proposed technology is set forth by an interdisciplinary partnership spanning the entire CSP value chain, comprised of leading research centres, universities, innovative SMEs and large enterprises, including ancillary services providers and technology end-users.

Deutsches Zentrum fuer Luft- und Raumfahrt e.V., **DLR**	DE	DLR
Centre for Research & Technology Hellas, **CERTH**	EL	CERTH CENTRE FOR RESEARCH & TECHNOLOGY HELLAS
University of Twente, **UT**	NL	UNIVERSITY OF TWENTE.
Fundación CENER, **CENER**	ES	CENER NATIONAL RENEWABLE ENERGY CENTRE ADItech
Fundación TEKNIKER, **TEKN**	ES	Tekniker
Fraunhofer Gesellschaft zur Foerderung der angewandten Forschung e.V., **FHG (IWKS)**	DE	Fraunhofer IWKS
DESTINUS Energy BV**, DEST**	NL	Destinus
KRAFTBLOCK GmbH, **KB**	DE	KRAFT BLOCK
LANDSON Emission Technologies A/S, **LET**	DK	landson
COBRA Instalaciones y Servicios S.A., **COBRA**	ES	cobra

Table of Contents

This deliverable is part of a project that has received funding from the European Union's Horizon Europe research and innovation programme under grant agreement no 101084569

Executive Summary

This document presents the design process of the porous matrices used in the regenerative system of the ABCSPF project plant approach, covering both the full-scale configuration and its downscaled prototype version to be realized in the frame of the project's lifecycle. The work is structured around the technical specifications that guide the design, the modelling tools employed, the definition of the real-scale matrix, the prototype adaptation strategy, and a sensitivity analysis of key design parameters.

The design is driven by system-level requirements such as maximum allowable pressure drop, operating temperatures and pressures, flow distribution homogeneity, and the need to achieve high efficiency and effectiveness as a heat exchanger. Two complementary modelling approaches were used: a dynamic system-level model developed in Dymola® and detailed CFD simulations, allowing for both performance evaluation and flow distribution analysis within the structured matrix.

The real-scale design work focused on defining the overall geometry and internal configuration of the matrix based on the imposed specifications and supported by numerical modelling. Different design alternatives were explored and analysed, taking into account operational feasibility and integration constraints at the system level.

For the prototype-scale design, the full-scale configuration was used as a reference, adapting it to the constraints and objectives of experimental testing. The work involved defining a representative geometry, preserving key operational parameters, and ensuring sufficient flexibility to test multiple configurations and materials.

Finally, a sensitivity analysis was conducted on certain parameters that are currently defined as design constraints but could be adjusted in the future to improve system performance. In particular, the cell density, as expressed by the CPSI (cells per square inch) parameter, in the porous honeycomb-like structures and the maximum allowable charging outlet temperature were evaluated, revealing clear opportunities for optimization in subsequent design iterations.

Changes with respect to the DoA

The delivery date has been delayed to provide the necessary time for the study and elaboration of as many as possible input properties of the investigated redox materials and structures, needed for the development of the regenerative matrix design.

1. Introduction

The plant concept in which ABCSPF is based builds upon the previous work carried out in the CAPTure project, which focused on the development of specific components for a high-efficiency, low-LCOE concentrating solar power (CSP) plant concept based on a Brayton cycle. This involved the design of a **fixed dual-bed regenerative system** ([1][2][3][4]) that enabled the thermal coupling between the atmospheric air receiver and the pressurized air gas turbine operating on a Brayton cycle.

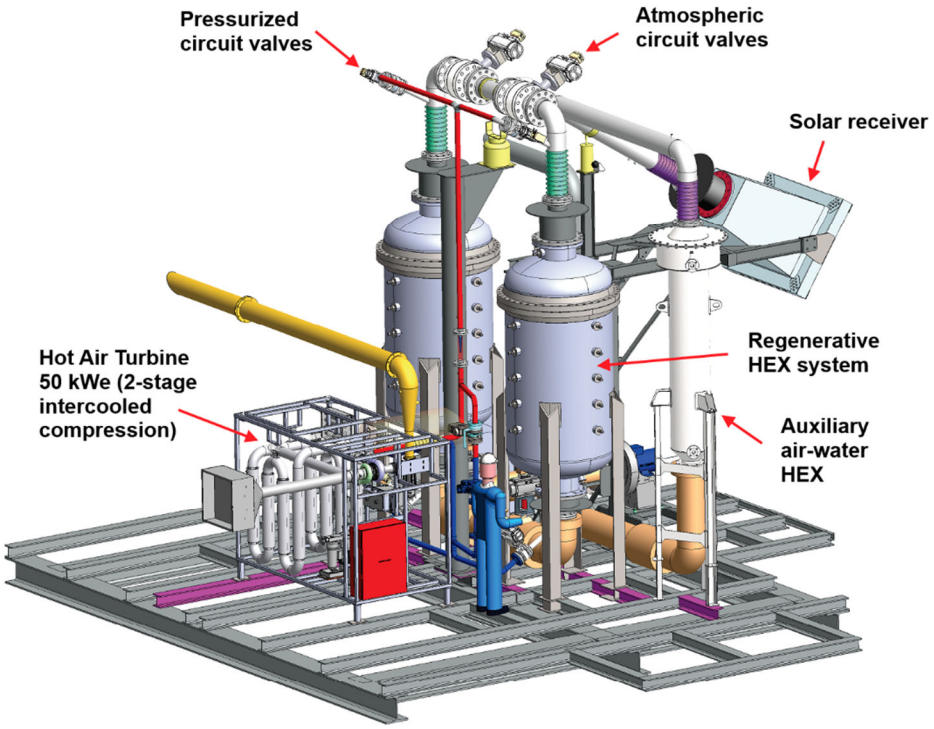

Figure 1: CAPTure Prototype CAD 3-D view

ABCSPF project aims to take this concept a step further by using redox material structures in the regenerative beds (instead of purely sensible ones). This is expected to improve the energy density and potentially provide a thermal boost that could increase the turbine inlet temperature and, as a result, its efficiency.

The following figures show the ABCSPF plant configuration, including the receiver, Brayton Cycle turbine, low and high temperature storage units, and the regenerative system (zoom).

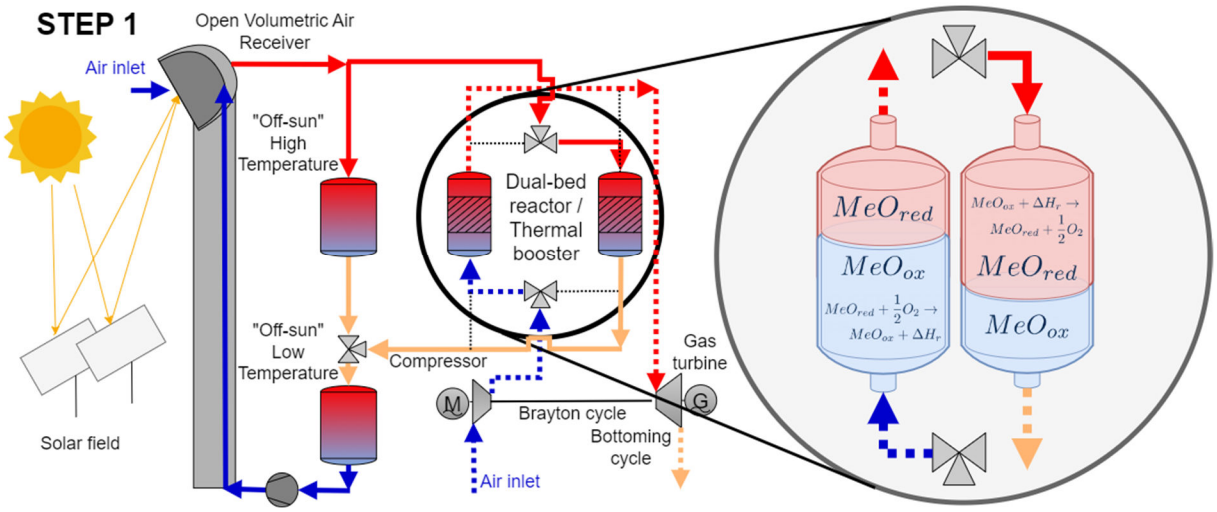

Figure 2: Operation mode 1 in ABCSPF concept

Figure 2 (Step 1) represents the **on-sun operation during the day**. There part of the hot air from the solar receiver (at atmospheric pressure) is sent to the charging bed (right chamber) to sensibly heat the ceramic material and, if thermochemical materials are present, trigger an **endothermic reduction reaction**. Meanwhile, another portion of the hot air is sent to storage to accumulate thermal energy for later use (off-sun operation). At the same time, the discharging bed (left chamber) receives cold pressurized air from the turbine compressor; as this air flows through the hot solid, it is heated sensibly and, if redox materials are present, also via the **provision of an additional heat coming from the exothermic oxidation reaction**. This hot, pressurized air is then sent to the gas turbine to generate electricity. During the night or when solar radiation is absent (off-sun operation), the heat stored in the storage blocks is used to heat the air instead of the receiver.

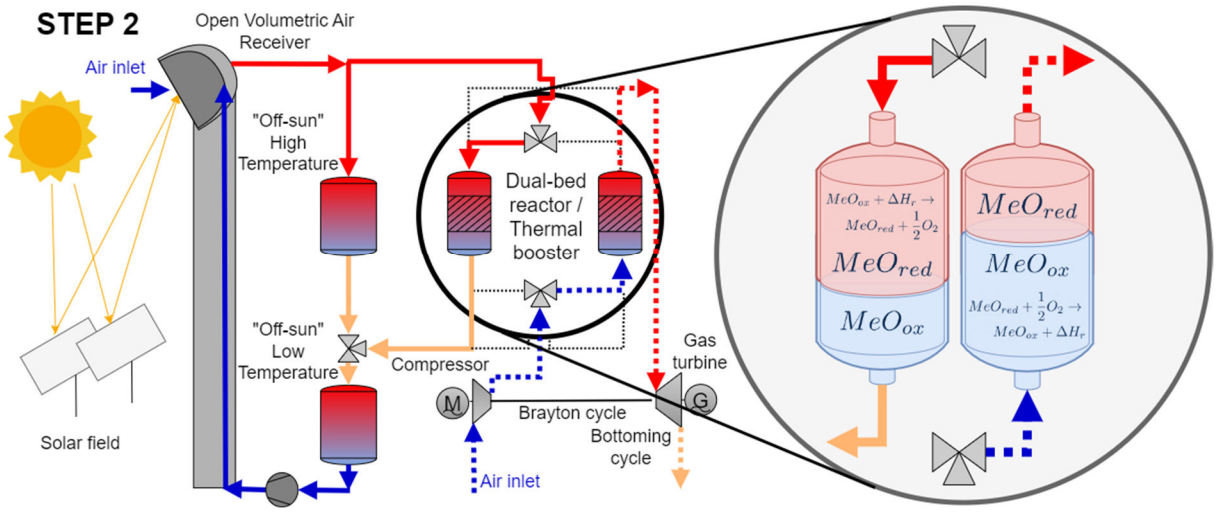

Figure 3: Operation mode 2 in ABCSPF concept

In Step 2 (see Figure 3), the roles of the two beds are switched: the one that was discharging now starts charging with hot air from the receiver, and the one that was charging begins to discharge by heating compressed air going to the turbine. Charging is always performed at atmospheric pressure, and discharging at pressurized conditions, which means both beds must be designed to handle pressure. This switching cycle allows the plant to supply hot air to the turbine continuously.

The following sections present a detailed design of the regenerative matrices, based on the results obtained in WP3 concerning viable sensible and thermochemical structures. This design is developed in accordance with the operating conditions imposed by the various operational modes, with particular emphasis on the integration of the regenerative system with the receiver/storage unit and the turbine

2. Specifications

The requirements for the design of the regenerative beds are structured in two groups:

- Available Materials and Structures
- Global system Operational Conditions

2.1. Available Materials and Structures

At the point of the starting of the design process, the most promising **redox structure for the regenerative beds is the $Ca_{0.90}Sr_{0.10}MnO_3$** (from now on CS10MO) composition shaped by extrusion into a honeycomb geometry of a relatively high density so that the energy density potential will be appreciable and in particular exceeding the targeted value of 300kWh.m^{-3} for the pre-defined 300-1100ºC temperature range. As already reported in D3.2, the targeted hybrid sensible/redox thermochemical approach for the regenerative system of ABCSPF is largely defined by the reaction enthalpy (ΔH_{rxn}) of its cyclic chemical redox reaction, which, for the specific case of CS10MO follows a non-stoichiometric scheme written as:

$$Ca_{0.90}Sr_{0.10}MnO_3 \leftrightarrow Ca_{0.90}Sr_{0.10}MnO_{3-\delta} + \tfrac{1}{2}\cdot\delta\ O_2 \qquad \Delta H_{rxn} \qquad (1)$$

The relevant physical, thermal and chemical properties of this type of structure as measured by the project partners in the frame of WP3 activities are the following:

- Channel shape Tetragonal
- Channel density 59cpsi
- Bed porosity 30%

- Bulk Density 2.10 g/cc
- Specific heat -6.4100E-10T^3 + 1.1700E-06T^2 + 1.6595E-04T + 8.7250E-01 J/gK (T ºC)
- Thermal conductivity 2 W/mK

Regarding chemical properties, the most important parameters are the **reaction rate dδ/dt**, and the **effective reaction enthalpy value $\Delta H_{rxn,effective}$.** Expressions for the reaction rates have been elaborated and validated vs. experimental results by partner CERTH in WP3 (Task 3.3) and are provided below:

$$\frac{d\delta(t)}{dt} = Rate_{red} + Rate_{ox}$$

$$\text{Reduction}: \left.\frac{d\delta(t)}{dt}\right|_{red} = Rate_{red} = k_{0_{red}} \exp\left(-\frac{E_{A,red}}{R\,T}\right)$$

$$E_{A,red} = E_{A,0,red} + c_{red}\,\delta^{\delta exp_{red}}$$

$$\text{Oxidation}: \left.\frac{d\delta(t)}{dt}\right|_{ox} = Rate_{ox} = -\,k_{0_{ox}}\,{Y_{ox}}^{yexp}\,\exp\left(-\frac{E_{A,ox}}{R\,T}\right)$$

$$E_{A,ox} = E_{A,0,ox} - c_{ox}\,\delta^{\delta exp_{ox}}$$

where k_{ox} and k_{red} [s^{-1}] are the pre-exponential factors, Y_{ox} [mol_{O2} mol_{gas}^{-1}] is the instantaneous oxygen molar fraction in the process gas, E_A [J mol^{-1}] the activation energy, R [J mol^{-1} K^{-1}] is the gas constant, T [K] is the substrate temperature, E_A [J mol^{-1}] is the activation energy at low temperatures or at zero δ values and c [J mol^{-1}] and δexp [-] are constants that correlate the effect of δ on the activation energy. It must be mentioned that although relatively complete, at the time for the preparation of the present deliverable the redox kinetic model was still in the process of refinement with additional experimental data and will continue to evolve as more experimental data are derived (included the ones with the project's small prototype system).

Reduction reaction				**Oxidation reaction**				
$k_{0,red}$ [s^{-1}]	$E_{A,0,red}$ [J mol^{-1}]	c_{ox} [J mol^{-1}]	δexp_{red} [-]	$k_{0,ox}$ [s^{-1}]	$E_{A,0,ox}$ [J mol^{-1}]	c_{ox} [J mol^{-1}]	δexp_{ox} [-]	$yexp$ [-]
$3.05 \cdot 10^{17}$	332000	492000	0.6	$2 \cdot 10^{14}$	267500	-400000	0.63	1

Table 1: Kinetic reaction parameters

The dependence of the effective reaction enthalpy on the non-stoichiometry factor δ (which in turns depends on the reaction temperature) is shown in Figure 3 (D3.2). The extent of reduction reaction, as indicated by δ, increases monotonically with the temperature and at 1100°C the non-stoichiometry factor reaches a value of approximately 0.12. Obviously, the higher the value of δ during reduction the higher the value of $\Delta H_{rxn,effective}$ in the course of the subsequent oxidation step

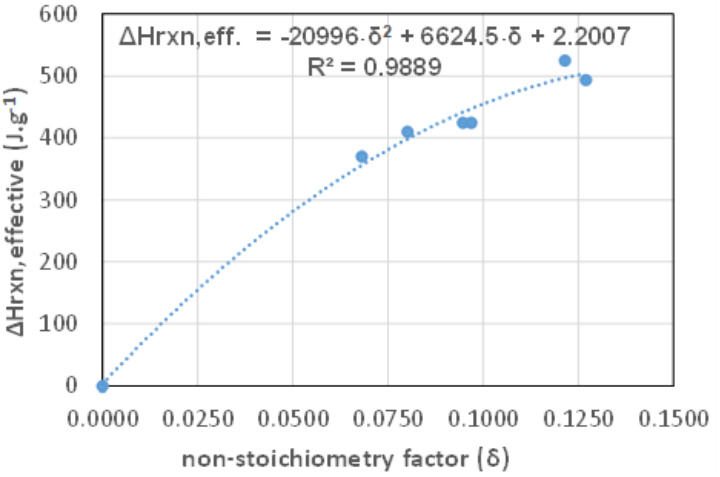

Figure 4: Enthalpy of reaction as a function of δ

At this stage of model development, weight variation in the material due to redox process is neglected. This variation is anyway quite limited; i.e. approximately 1.5% for δ = 0.125.

Related to the **sensible materials** worked out in the project, the properties of the most promising one (OS1) have been determined as follows:

Same shape as the redox structure:

- Channel shape Tetragonal
- Channel density 59cpsi
- Bed porosity 30%

- Bulk Density 1.40 g/cc
- Specific heat 3.6349·10-10·T^3 - 9.9385·10-7·T^2 + 1.1637·10-3·T + 5.9209·10-1 J/gK (T ºC)
- Thermal conductivity 0.5 W/mK

2.2. Operational Conditions

These requirements are mainly referred to the connection of the regenerative system to both the receiver/storage system (charge) and the turbine (discharge) as shown in Figure 2.

These connection conditions refer mainly to the temperature and mass flow rate of the flow coming from the receiver/storage, required by the turbine and are closely related to the operation modes of the plant.

During the day (sun hours) the regenerative system will be receiving a **constant temperature air flow at 975ºC** and variable mass flow rate from the receiver. However, during off-sun hours the storage will provide the necessary energy, and the system will work with constant mass flow rate and **variable supply temperature**.

Another restriction coming from the connection to the receiver is that related to the allowable pressure drop through the charging bed. As it has been decided to keep the plant auxiliary consumption below 10%, relevant calculations by partner CENER have indicated that this corresponds to a maximum **pressure drop in this bed of 5000Pa**.

Moreover, also coming from the configuration of the plant, specifically from the design of the low temperature storage (see Figure 1), a **maximum temperature of 500ºC at the outlet of the charging bed** is established, according to the configuration of the plant storage system.

Related to the connection of the regenerative system with the turbine, these conditions come from the corresponding **turbine operating curves** that establish the value of mass flow rates and temperatures for different turbine loads (partner DES).

In this case two different turbines have been studied, corresponding to two different electric power levels (**20MWe, 1.5MWe**).

Load (%)	Compressor inlet flow (kg/s)	Compressor Exit Press P3 (kPa)	Compressor Exit Temp T3 (ºC)	Turbine rotor inlet temperature (ºC)
25	64.39	1328.30	432.22	762.53
50	66.03	1405.24	439.17	893.50
75	70.15	1532.78	449.13	1007.88
100	82.50	1823.85	476.40	1079.70

Table 2: 20MWe Destinus Turbine Performance Map

Load (%)	Compressor inlet flow (kg/s)	Compressor Exit Press P3 (kPa)	Compressor Exit Temp T3 (ºC)	Turbine rotor inlet temperature (ºC)
25	7.10	947.10	346.93	663.40
50	7.10	991.40	351.36	769.50
75	7.00	1029.50	354.97	873.61
100	6.90	1063.90	358.31	979.23

Table 3: 1.5MWe Destinus Turbine Performance Map

3. Design Tools

This chapter presents the main modelling approaches used to support the design and optimisation of the hybrid sensible–thermochemical storage system. Two complementary methodologies are employed: a dynamic system-level model developed in Dymola for simulating the overall behaviour and control of the storage unit, and Computational Fluid Dynamics (CFD) for detailed analysis of fluid flow within the reactor. Together, these tools provide a comprehensive understanding of the system's thermal and hydraulic performance, guiding the development of an efficient and robust reactor design.

3.1 Dymola Model

A Dymola dynamic model has been developed to support the conceptual design and system specification of a hybrid sensible–thermochemical storage (TCS) pressurized unit for thermal boosting operation. The modelling work focuses on adapting the previously developed sensible-only fixed bed design from the CAPTure project to include thermochemical processes under pressurized conditions.

Two different models have been developed to simulate and analyse the system under various operating conditions. The first one is a single-bed model, which allows for detailed analysis of the charging and discharging processes independently. This model is particularly useful for testing the thermal behaviour of the system under different boundary conditions, such as varying air inlet and solid temperatures, pressures, and mass flow rates.

The second model shown in Figure 5 consists of two beds working in parallel, representing a more realistic operation mode of the full system. These two beds operate synchronously, with a control algorithm implemented to alternate charging and discharging between them. This enables the simulation of continuous operation and provides a better understanding of the dynamic performance of the system, including switching logic, thermal cycling, and interaction with external components like the turbine control.

In both cases, the regenerator model includes some simplifications. The fluid is assumed to be uniformly distributed throughout the flow channels, which allows for a one-dimensional treatment of the flow. The bed is considered adiabatic, meaning that heat exchange with the environment is not taken into account. Additionally, temperature variation is only considered in the longitudinal direction, neglecting any radial temperature gradients within the solid material.

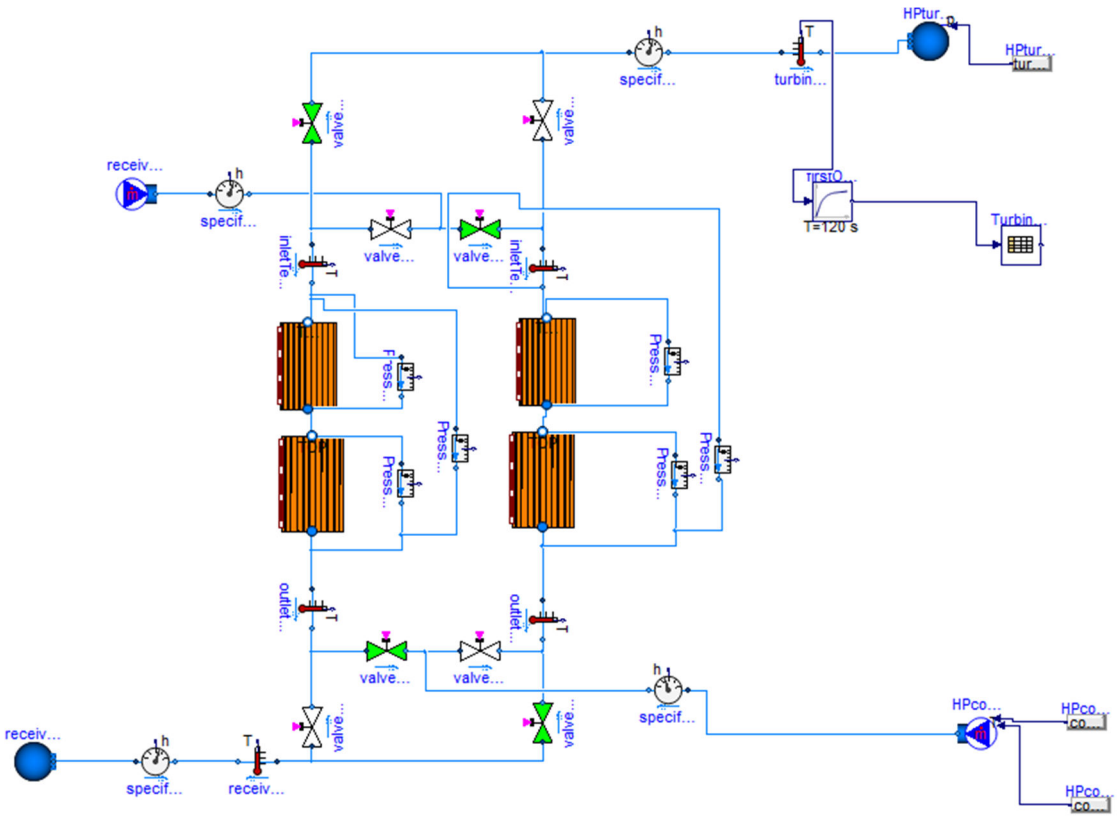

Figure 5: Dual-bed model Dymola scheme

3.2 Computational Fluid Dynamics (CFD)

In addition to the reactor models developed in Dymola for system-level design and dynamic simulation, Computational Fluid Dynamics (CFD) has been introduced as complementary tool to support the detailed design of dual-bed reactor, focused on the analysis of the fluid-dynamic behaviour. This enables the analysis of local phenomena – such as recirculation zones, hotspots, and pressure drop – that cannot be captured by system-level models. This level of detail is essential for optimising the geometry of the reactor, improving thermal management, and enhancing overall efficiency.

By concentrating on fluid dynamics, the study aims to characterise flow patterns and velocity fields, providing critical input to support optimal reactor design and operation.

A real-scale-bed CFD model has been developed to support the reactor design process. It consists of multiple honeycomb structures but does not model the individual channels in detail due to their large number, as detailed resolution is computationally infeasible. Instead, it employs porous media models to represent the honeycombs, enabling efficient and computationally less expensive analysis of fluid flow distribution along and across the reactor.

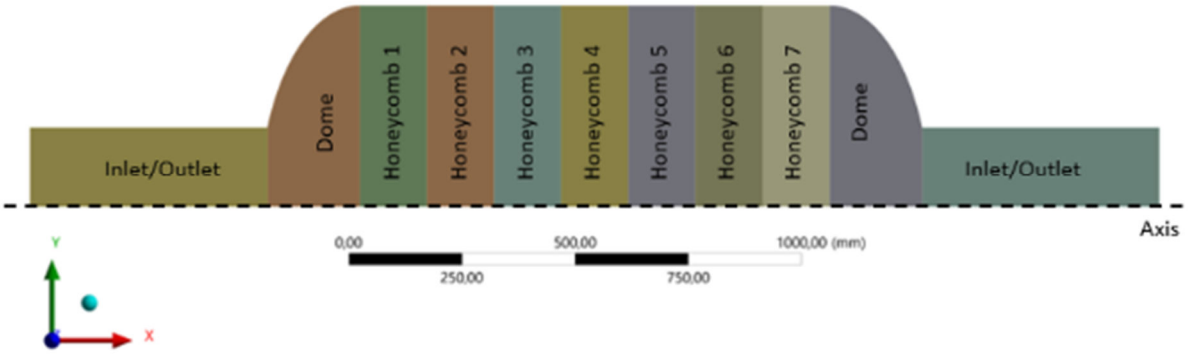

Figure 6: Reactor geometry and segmentation of computational domain for CFD analysis

The CFD study contributes directly to the reactor design process by providing insights into fluid flow distribution and identifying potential areas for optimisation. This work ensures a comprehensive understanding of flow distribution, contributing to the overall design optimisation and validation of the reactor concept within the scope of the project.

4. Real Scale Dual-Bed Regenerative Matrix Design

The design of the Dual-Bed Regenerative Matrices is tackled according to the described specifications and with the assistance of the described tools.

The purpose of the design is to establish the optimum regenerative beds global dimensions (diameter and length) and the configuration of the different types of available structures (redox and sensible) inside.

4.1 First Steps in the Design Process

Focusing on the design of the regenerative beds, the bed dimensions of the CAPTure project are selected as starting point (Ø0.85m, Length 1.5m), and with them the first complete model simulations are carried out, with the same mass flow rate for the charging air flow as in CAPTure (0.4kg/s) but the updated temperature (975ºC instead of 900ºC for charging and around 400ºC from the 20MWe turbine to discharge instead of 275ºC), material (CS10MO redox structures instead of only sensible cordierite), and discharging pressure (18bar instead of 10bar).

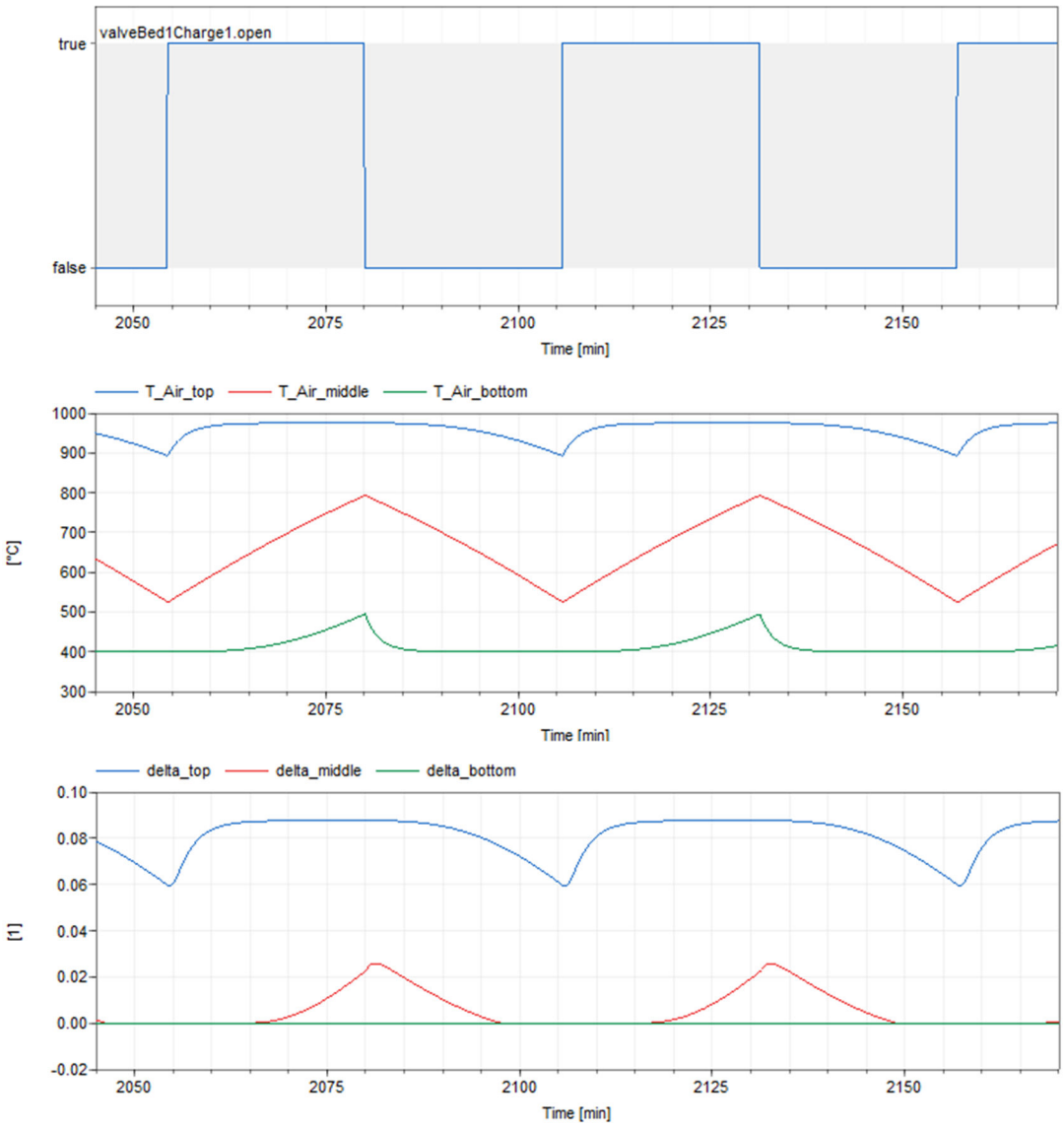

Figure 7: Simulation results of Ø0.85m and length 1.5m regenerative bed during switching conditions

The results shown in Figure 7 correspond to one of the regenerative beds. The graphs display simulation results during the stabilized phase of the cycle, omitting the disturbances observed during the initial minutes, which are attributed to the effect of the simulation's initial conditions.

The first graph indicates the periods during which the chamber is in charging mode (true) and discharging mode (false), based on the position of the corresponding charging valve. There it can be observed that the duration of the cycle for the simulated conditions is around 25min; nearly an increase of 50% in comparison to the duration in the CAPTure project (17min).

The second graph shows the evolution of air temperature in three different zones: the lower section (when charging: the air exiting the bed towards the low temperature storage; when discharging: the air coming from the turbine compressor to the

regenerative bed), the middle section, and the upper section (where air enters from the storage/receiver during charging and exits toward the turbine during discharging).The third graph presents the evolution of the solid-phase delta value in those same locations.

Additionally, with the simulation data the following graph of Figure 8 has been worked out, showing the distribution of the temperature at the bed along its length during the charging process at three different moments: charge process just initiated, charge process finished and about to switch chambers, and a moment in between these ones.

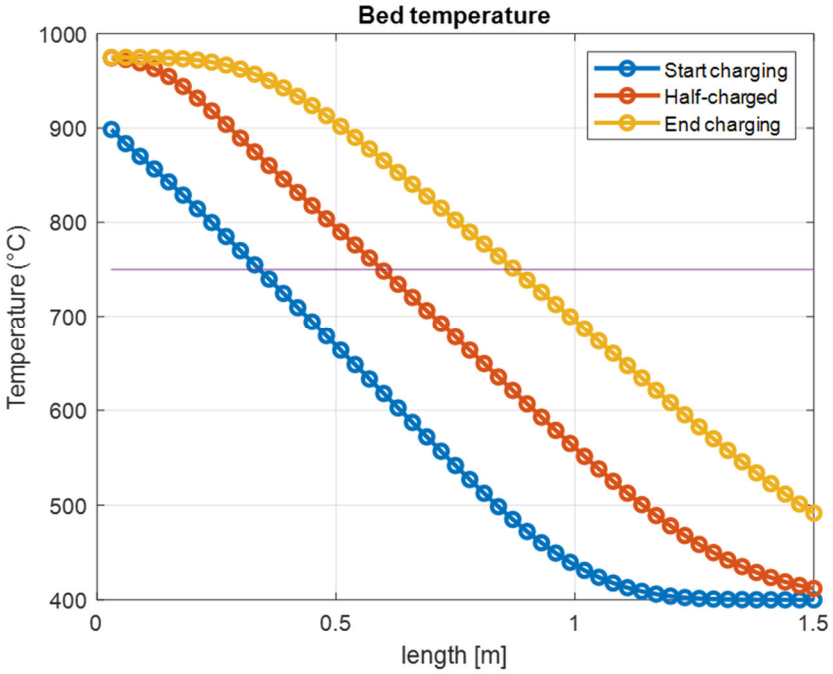

Figure 8: Thermocline in the 1.5m bed at three different moments

These previous graphs allow us to establish some preliminary conclusions:

- Thermocline profile (Figure 8): the way the system is operated along with the boundary conditions causes the temperature distribution in the bed to resemble a thermocline. It can be observed that during charging the nominal temperature (975ºC) is only achieved at the top part of the bed, and that chemical energy is only stored in half of the bed.
- At Figure 8, it can be observed that the minimum air temperature at the outlet is around 900ºC, which involves a quite high mean outlet temperature and thus a high value of the efficacy and efficiency as heat exchanger.
- At Figure 8 no temperature boosting effect is observed; the chemical energy is slowly released as expected under the operation conditions imposed by the system configuration itself (continuous connection to the receiver and turbine). However, this chemical energy release allows for a longer cycle time in comparison with the CAPTure only sensible design, and a slightly higher mean discharge temperature.

All these results serve as a good starting point upon which the system design can be further refined and optimized. However, the high-level differences between CAPTure project plant and the ABCSPF plant concept have to be considered, as shown in the following chart:

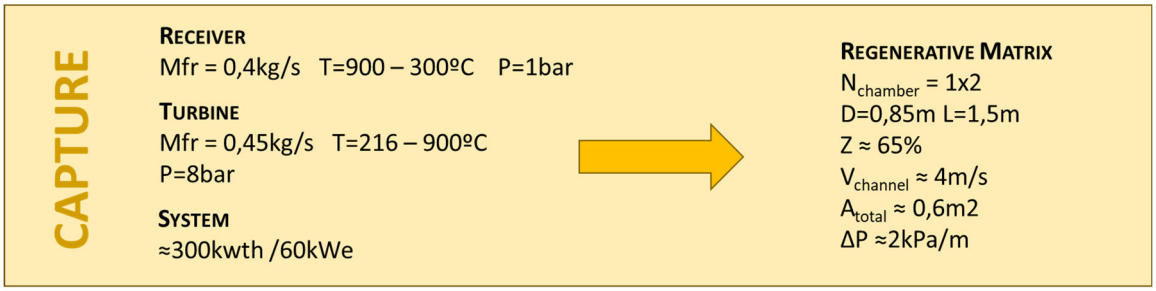

Figure 9: CAPTURE plant conditions

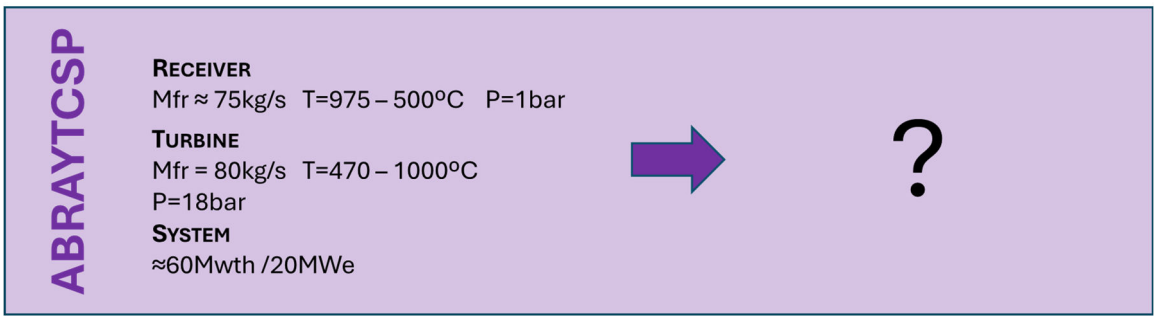

Figure 10: AbraytCSP plant conditions

As included in the specification section, there is a **maximum pressure loss value during charging of about 5000Pa**. This stems from the plant configuration established for the project and the requirement to move air through the receiver–storage–regenerative circuit, while keeping auxiliary energy consumption below 10%.

Taking into consideration the way the bed is modelled, the maximum air mass flow rate for the charging (and a bed Ø0.83m) corresponding to those 5000Pa can be calculated. This value depends on the length of the bed, and **results around 0.48kg/s for a 1.5m length.**

The big difference between CAPTure System and ABCSPF system is the total power: 60kWe vs 20MWe, and the corresponding air mass flow rate that has to be heated up by the regenerative system. This difference stems from the fact that the CAPTure system was a demo-size unit operating under real conditions, whereas the ABCSPF system is a scaled-up commercial-size plant designed for full-scale deployment.

To have an idea of the influence of the mass flow rate (air velocity per channel) and the bed length in the results, the dual bed thermochemical system (Ø0.83m each bed) has been simulated for **two different bed lengths and for several channel velocities at each length**, and the following results have been obtained. The velocity per channel and pressure loss of the following results correspond to those of atmospheric air (charging).

Case 1: Length 1.5 m, Ø0.83m			
	Case 1.1	Case 1.2	Case 1.3
m_flow [kg/s]	0,48	0,24	0,07
v_channel [m/s]	7,88	3,89	1,1
ΔP_charge [bar]	**0,05**	0,025	0,007

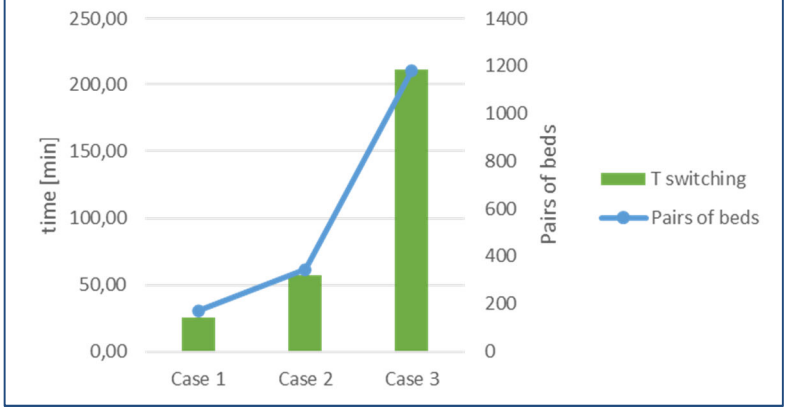

Figure 11: Case 1 results

Case 2: Length 0.5 m, Ø0.83m					
	Case 2.1	Case 2.2	Case 2.3	Case 2.4	Case 2.5
m_flow [kg/s]	1,35	0,675	0,48	0,24	0,07
v_channel [m/s]	22,6	11,2	7,88	3,9	1,1
ΔP_charge [bar]	**0,048**	0,024	0,017	0,008	0,0024

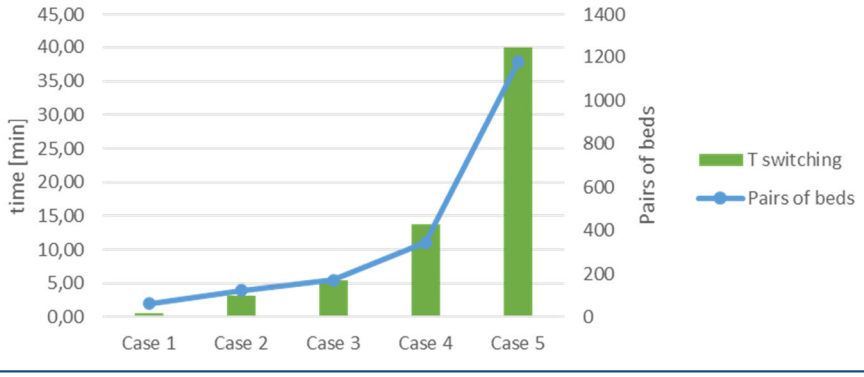

Figure 12: Case 2 results

When comparing the different simulations, the main differences appear in the duration of the cycle, and the total number of regenerative systems as a consequence of the used mass flow rate with respect to the total value imposed by the turbine. Variables such as the total stored energy, minimum outlet temperature, etc. seem to be very similar.

Longer cycle times involve more continuous operation of both the valves and the turbine (less number of switchings), this resulting in a higher life cycle. Additionally, longer cycle times with similar minimum outlet temperatures involve higher mean temperature at the outlet and thus higher efficacy.

Although there is no strict limitation on the maximum number of regenerative systems, experience from CAPTure project indicates that these are costly systems—primarily due to the high cost of components such as the vessels (which must withstand high temperatures and pressures), but especially because of the cost of valves, which must tolerate both high temperatures and pressure differentials. For this reason, a large number of regenerative systems could render the plant concept financially infeasible.

Cycle duration and the required number of regenerative systems are closely related: a longer cycle time implies a greater number of regenerative systems. However, it is not clear which of these two variables would have a greater influence on the design. What is clear, though, is that for the reference cycle time obtained in CAPTure (17 minutes), the number of regenerative systems required—regardless of the lengths analyzed—appears to be infeasible.

Another variable that could lead to a decrease in the number of regenerative systems is the bed's diameter. Again, there is not a maximum limitation specified, however, even with 3 times wider beds the resulting number of regenerative systems is too high for the best case identified (20 systems for 1.5 length).

4.2 Nominal Power Change

Taking these preliminary results into account, and upon re-evaluating the optimal plant configuration, it has been decided to revise the system's nominal power specification **from 20 MWe to 1.5 MWe**, as this is considered a more suitable value in light of the updated analysis. This scale corresponds exactly to the largest currently existing air-operated solar thermal power plant, Solar Tower Juelich (STJ), of DLR. Thus, it also makes sense to be pragmatic and focus on an existing, in-principle compatible system that ABCSPF technology could be scaled-up and tested at a pre-commercial scale.

The 1.5MWe turbine provides additional advantageous operational environment apart from the obviously lower total mass flow rate (6.9kg/s vs 82.5kg/s):

- Lower discharging temperature → higher temperature difference with the 500ºC charging outlet limitation → higher cycle duration
- Lower discharge pressure → lower implementation cost

Looking at the results obtained for L=1.5m and L=0.5m, a **new length of 1m** for the bed is proposed. To assess the suitability of this new length (and in principle Ø0.83m) with the new 1.5MWe turbine, simulations are carried out with **two different channel velocities** to also assess the possible influence of this parameter in the regenerative performance.

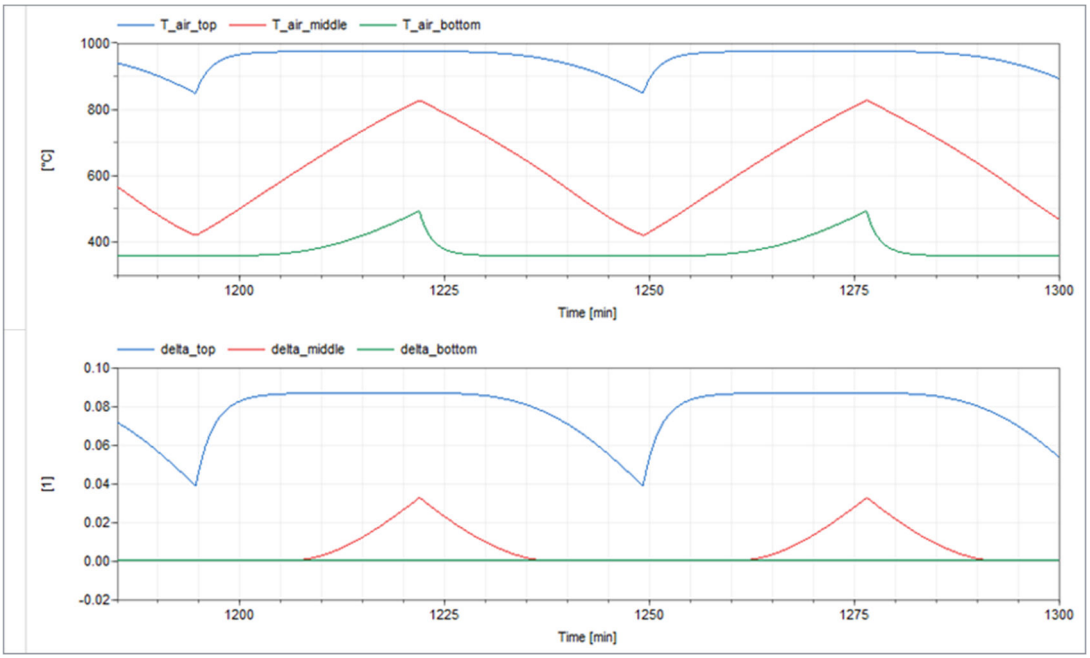

Figure 13: Simulation results in 6.4 m/s velocity case

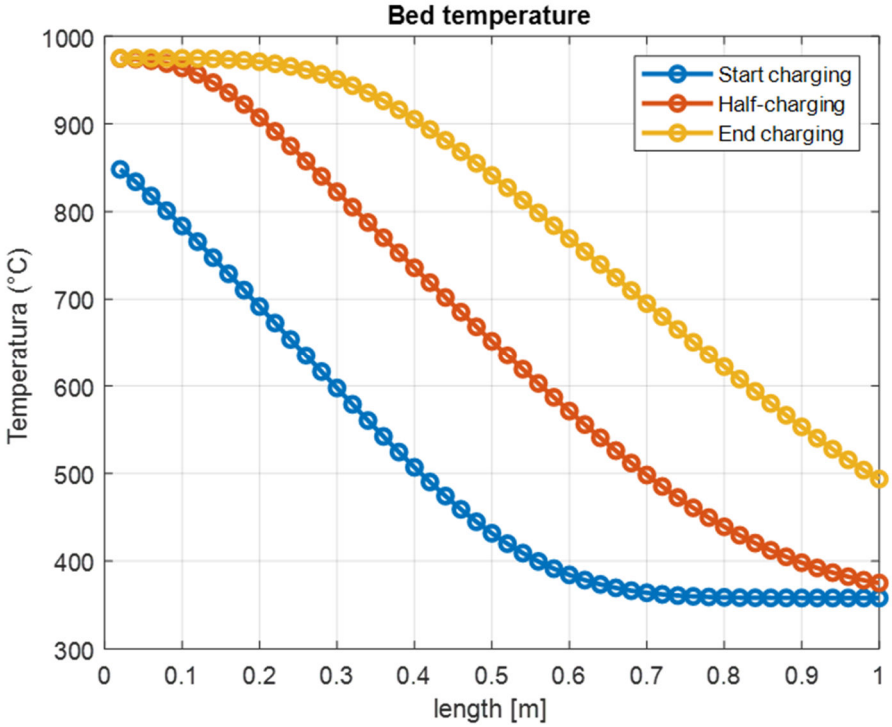

Figure 14: Thermocline in 6.4m/s velocity case

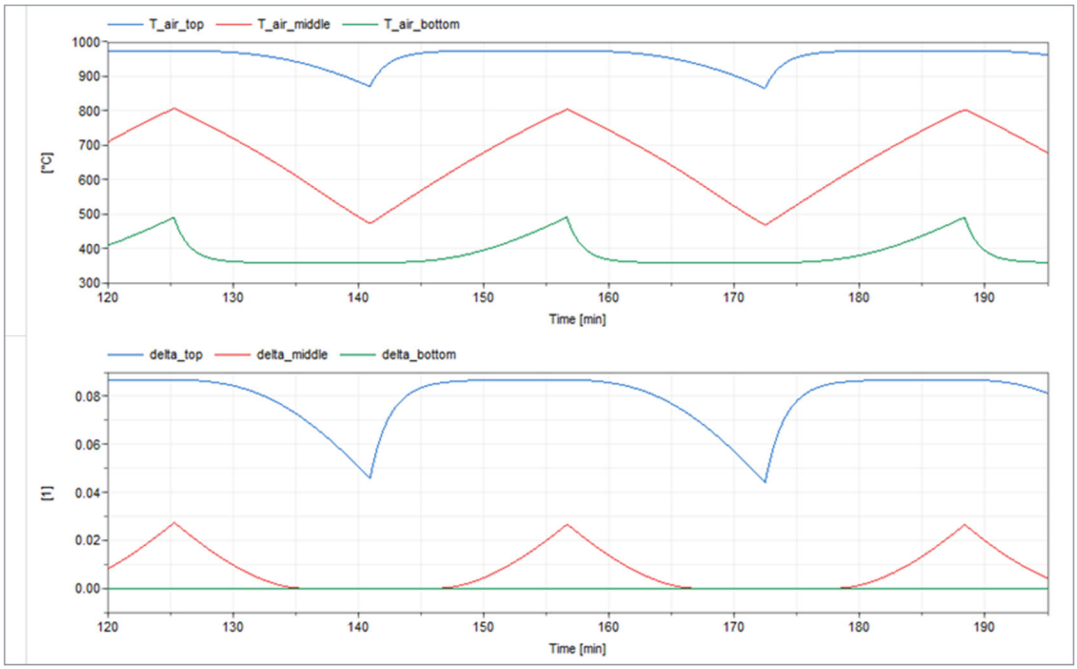

Figure 15: Simulation results in 9.5m/s maximum admissible velocity case

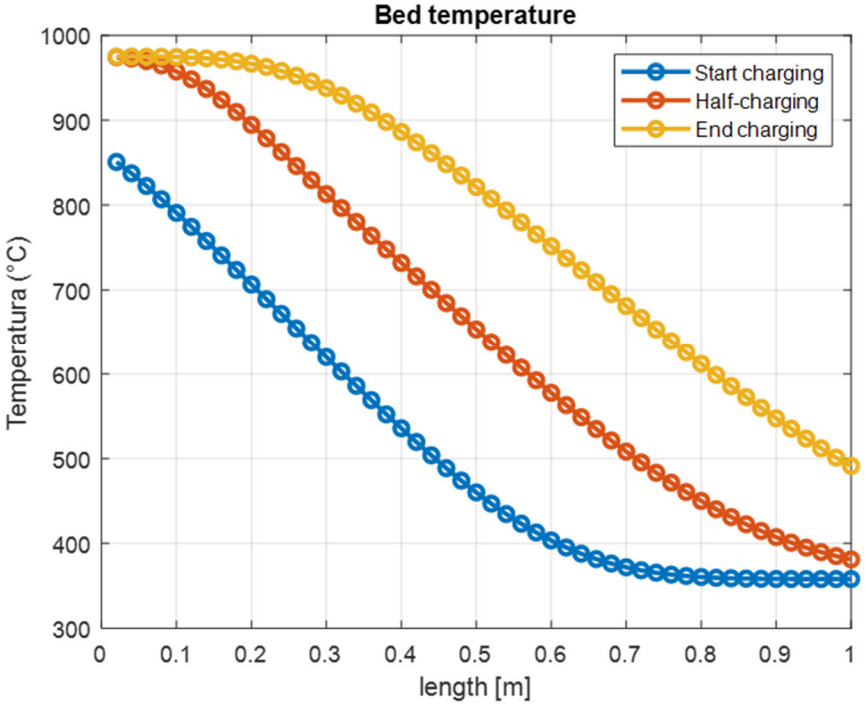

Figure 16: Thermocline in 9.5m/s maximum admissible velocity case

It can be observed that in both cases the thermoclines are very similar and so are the minimum outlet temperatures towards the turbine; hence it can be concluded that the velocity has no big impact either on the stored-released energy or on the efficacy.

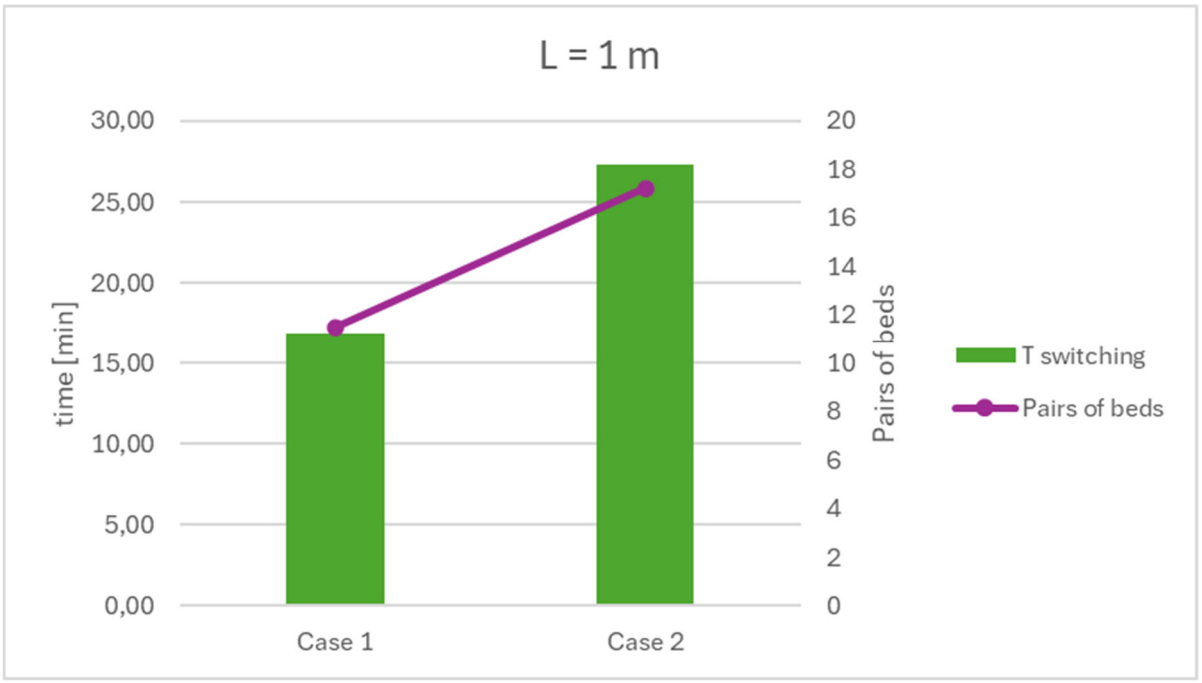

Figure 17: Switching time and number of beds in two cases

Again, the most affected parameter is the cycle time, that is around 17min for the maximum allowable velocity case (0.6kg/s per bed) and 27min for the lower velocity case (0.4kg/s per bed).

Regarding the number of regenerative systems, now for a 17min cycle time (similar value as that in the CAPTure project) 12 regenerative systems are needed. Furthermore, by increasing the bed diameter up to 3m**, it could be feasible to operate with just 1 regenerative system**.

In conclusion, it is established that a bed length of 1m provides optimum operating conditions for the system and keeps it committed to the specifications.

4.3 Combination with only sensible material inside the bed

Given that the thermochemical properties of the material are activated above 750 °C, and that—as shown in the thermocline in Figure 16 - nearly half of the bed length does not reach that temperature, it was decided to run simulations replacing that length of the chamber with purely sensible material, also developed within the project. The sensible-only structure has the same cpsi value as the CS10MO. The simulation results obtained are presented below.

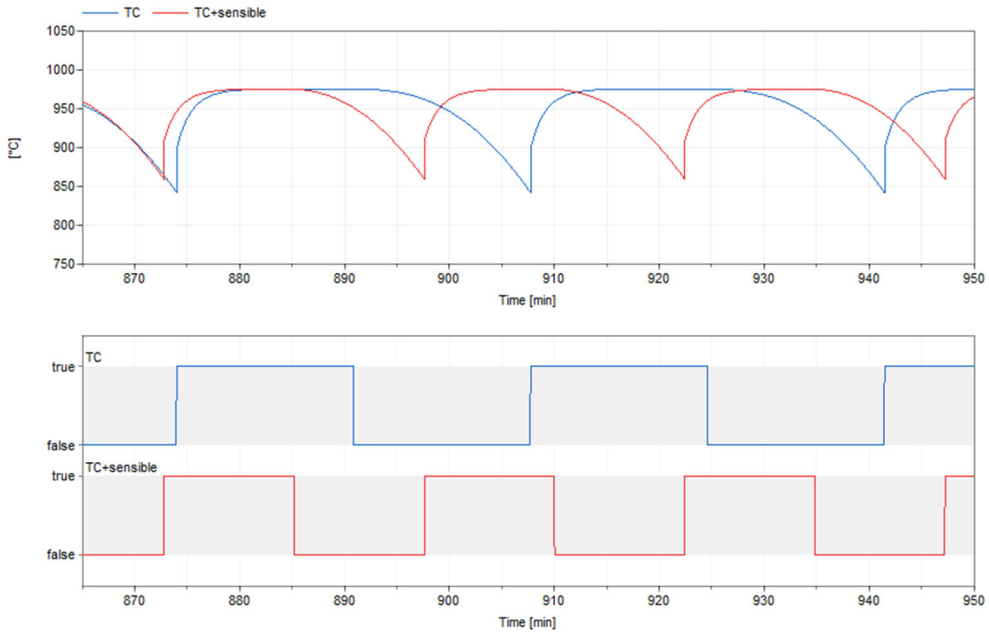

Figure 18: Simulation results in all bed TC vs bed TC+OS1 from the upper section of the regenerative bed

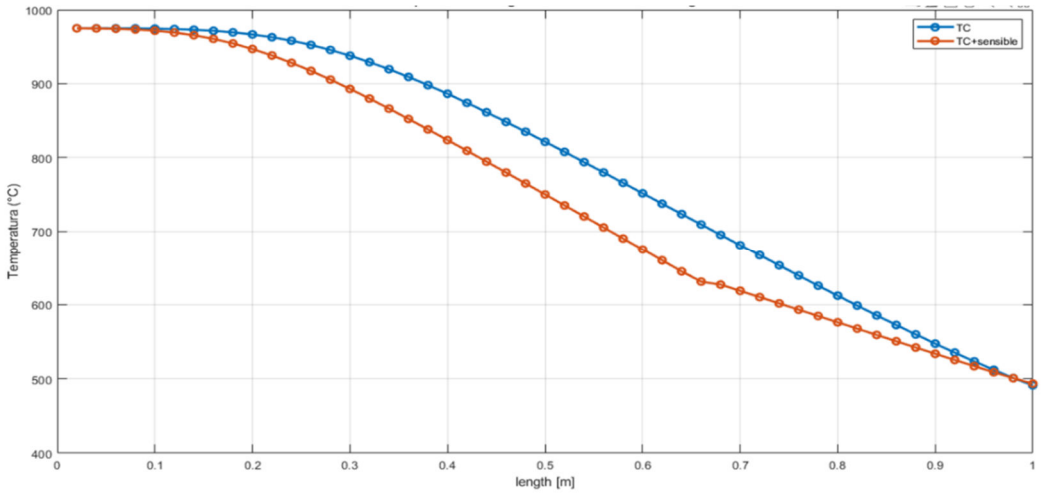

Figure 19: Thermocline in all bed TC vs bed TC+OS1 at the end of charging phase

As a result of this change the cycle duration is shorter (12.5min vs 17min) but the minimum outlet temperature is higher (858.4ºC vs 841.1ºC). Looking at the shape of the thermocline it can also be observed that the total stored energy (reached temperatures) is lower, that explaining the shortening of the cycle.

This is because the critical properties such as heat capacity and bulk density of the only sensible material are lower with respect to those of the redox thermochemical material. For the real scale design, it has to be decided if it is worth to work out this substitution of material, taking into account the materials cost.

4.4 Influence of the turbine control system

Until now, the calculations have been based on the assumption that the turbine's compressor supplies an air flow with constant mass flow rate and temperature. However, the turbine actually includes an internal control system through which these values vary depending on the inlet temperature from the regenerative system.

This variation affects the performance of the entire system, as both the operating point of the turbine and the thermal balance of the receiver/storage–regenerative loop are influenced by these changes. Consequently, to obtain more realistic results, it becomes necessary to incorporate this control behaviour into the simulation model, allowing for a dynamic response of the air flow rate and temperature according to the turbine's internal regulation strategy.

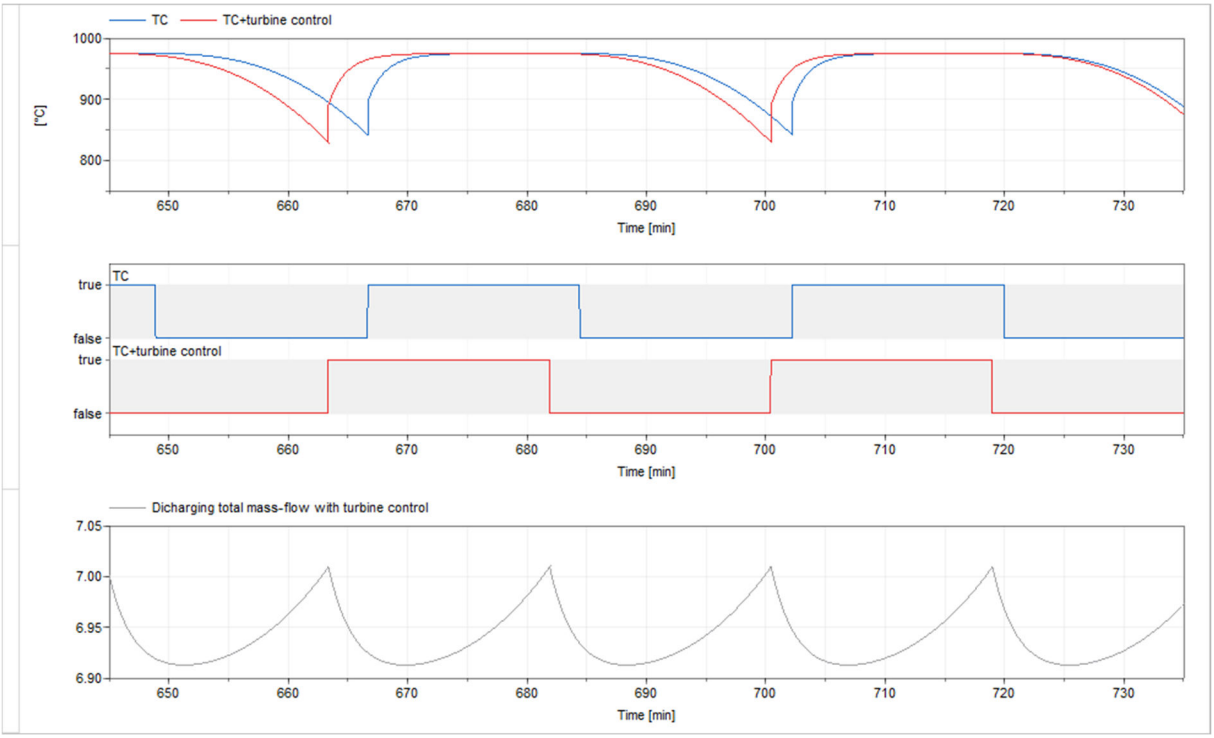

Figure 20: Simulations results in all TC without turbine control vs turbine control implementation

With the integrated turbine control, when the outlet air temperature during discharge starts to decrease, the system responds by increasing the discharge mass flow rate and reducing the air inlet temperature. This leads to cooling the regenerative bed more effectively. As a result, it takes longer to reheat the chamber during the charging phase, which increases the total cycle time. As can be seen in the previous graph, the longer duration of the discharging phase also causes the outlet air temperature to drop even more, compared to the case without turbine control.

Until now, a constant mass flow rate has been considered for both charging and discharging phases. However, when turbine control is introduced, the turbine flow rate increases as the inlet temperature decreases—which is precisely what occurs toward the

end of the discharge cycle. This creates an imbalance between the charging and discharging flow rates. Nonetheless, it has been observed that this does not compromise the stability of the system or the cyclic operation.

This is a positive outcome in view of future work focused on developing the control strategy for the regenerative system, where variations in the charging flow—due to changes in solar irradiance or the discharge of the thermal storage—will be taken into account.

4.5 Evaluation of Flow Uniformity Based on CFD Results

The following section presents the results obtained from the CFD simulations of the full-scale reactor model

These simulations aim to evaluate the flow behaviour and distribution within the complete geometry under realistic operating conditions derived from the system-level Dymola model. The analysis focuses specifically on the airflow distribution across the different honeycomb units, in assessing the uniformity and potential imbalances in the system. The following results are presented for both operating modes: charging and discharging, in order to evaluate and compare the flow distribution performance under each condition.

The model (see description in section 3.2), represents a bed of 1m length and a diameter of 0.83m, made up by thermochemical bricks. According to the specification, the cell density of the bricks is 59 cpsi, and the brick height is 150 mm. Thus, seven rows of bricks are modelled, which are actually equivalent to 1050 mm in length. Additionally, the reactor geometry includes two elliptical 2:1 heads (domes) at each end, designed according to ASME standards. Additionally, the reactor features two inlet/outlet pipes—one at each end, depending on the operating mode—whose dimensions were defined by DESTINUS and CENER based on velocity constraints for air transport. The pipe diameter was determined according to the most restrictive operating condition, resulting in a diameter of 355 mm

Due to manufacturing limitations, achieving perfect alignment between the channels of adjacent honeycomb bricks is nearly impossible. Consequently, in a real reactor configuration, support legs or gaps are introduced between the honeycombs. This approach is based on practical experience gained in the CAPTURE project (see Figure 22). To accurately represent this, additional CFD models have been developed where fluid regions are included between successive honeycomb bricks, simulating these gaps. This allows analysis of flow redistribution caused by the presence of support legs, which can significantly influence the overall flow distribution within the reactor.

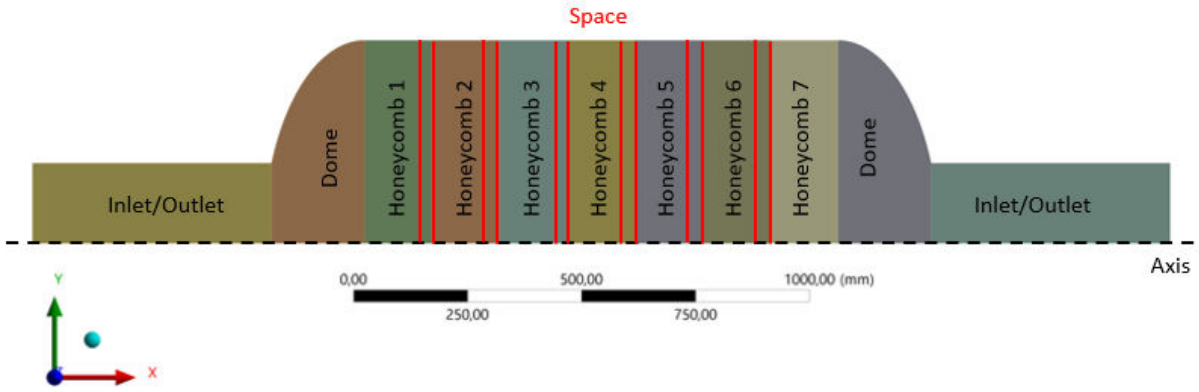

Figure 21: Reactor geometry and computational domain division including support leg gaps between honeycomb bricks.

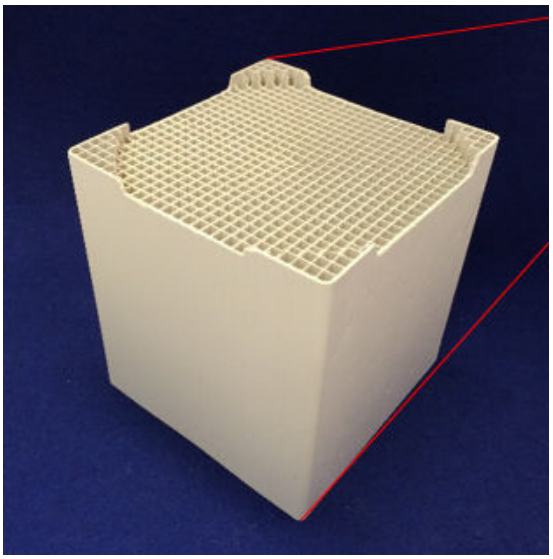

Figure 22: CAPTure sensible-only brick with "legs" allowing for a gap between rows

4.4.1. Charging Mode

The following figure presents the velocity contours for the charging mode under nominal flow conditions. The first case corresponds to the ideal configuration, in which perfect alignment between the honeycomb bricks (channels) is assumed—an unrealistic scenario given the practical assembling constraints. Misalignments between adjacent bricks are inevitable and therefore support legs or gaps must be introduced between them. To evaluate their impact on the internal flow distribution, a parametric study has been conducted by varying the size of the inter-brick gap from 0.5 mm to 35 mm. From the velocity contours shown in Figure 23, the redistribution of the airflow inside the reactor due to these gaps can be clearly observed.

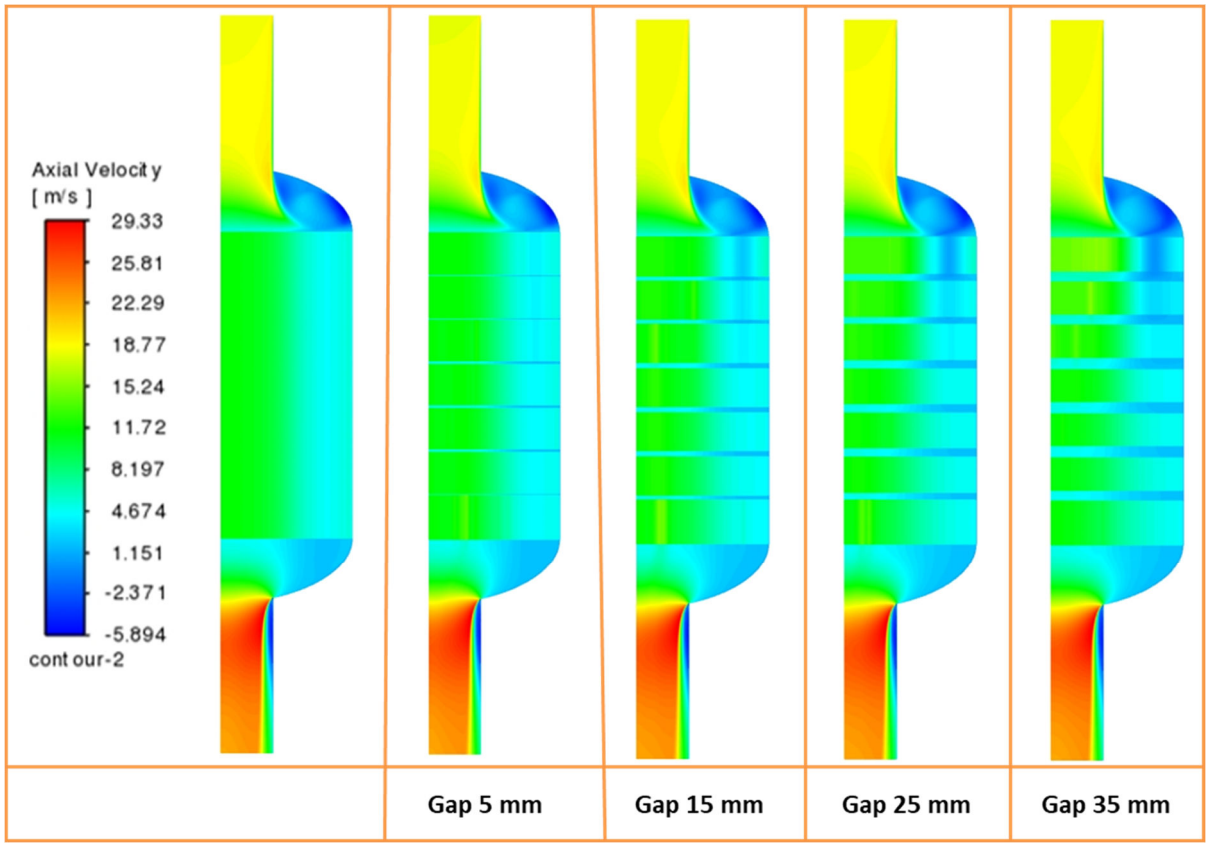

Figure 23: Velocity contours for charging mode at different gap sizes.

These velocity contours are further quantified through the calculation of the uniformity index, providing a numerical measure of flow distribution quality. The corresponding uniformity index graphs are presented in Figure 24 , allowing for a detailed comparison of flow homogeneity across the different gap sizes considered.

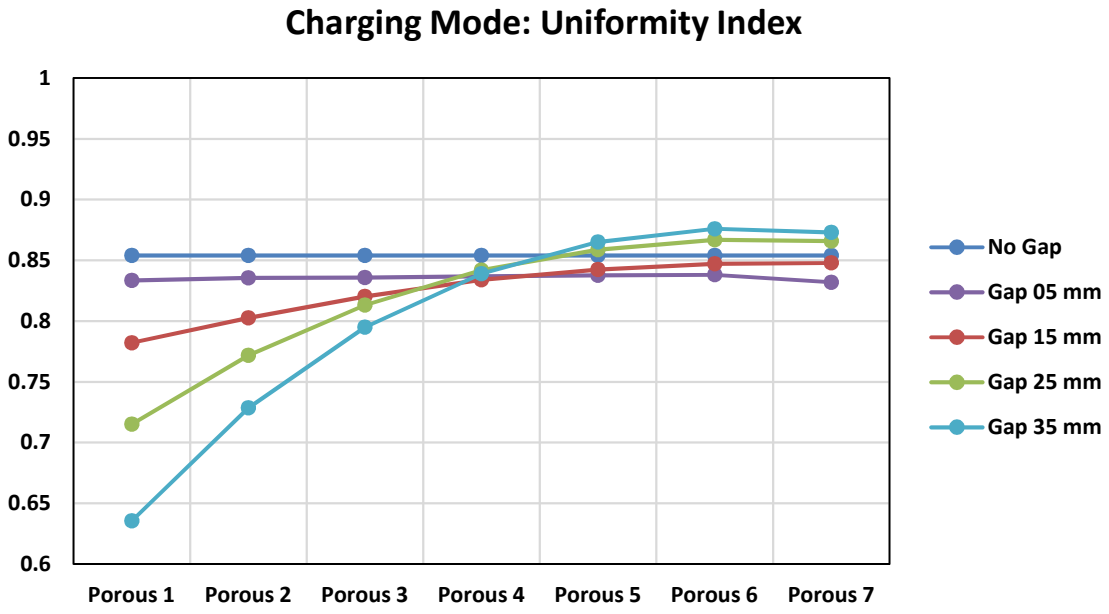

Figure 24: Uniformity index in each 7 honeycombs along the reactor for varying gap sizes in charging mode.

By comparing the values across different gap configurations, it is possible to evaluate the impact of structural spacing on flow homogeneity and identify configurations that promote optimal reactor performance.

In the ideal case of no gap, the uniformity index is approximately 0.85, which is generally considered a low value indicating suboptimal flow uniformity. For a small gap of 0.5 mm, the uniformity index remains close to this ideal value.

As the gap size increases, the flow uniformity near the reactor inlet decreases significantly, resulting in a much less uniform velocity distribution in the initial section of the reactor. However, as the fluid progresses through the reactor and passes the gaps, the flow gradually becomes more homogeneous. Notably, downstream of these regions, the uniformity index improves, even exceeding the ideal baseline value. This behaviour highlights the impact of larger gaps on flow maldistribution near the inlet, while also demonstrating the reactor's capacity to partially re-establish flow uniformity further along its length.

These results suggest that an optimal reactor design should aim to minimize the gap between honeycomb sections as much as possible. The final gap size will ultimately be determined by the manufacturing tolerances and capabilities of the supplier. Keeping the gap to a minimum is crucial to ensure a more uniform flow distribution and thus maximize reactor performance.

However, when comparing these uniformity values with those reported in the Capture project, it is evident that the current values are significantly lower. This discrepancy is likely due to the lower cell density (cpsi value) in the present designs, which can impact the flow uniformity within the reactor. Thus, a sensitivity analysis of this parameter has been conducted (see section 6.1) and is discussed in detail in a later section.

4.4.2. Discharging Mode

In discharging mode, the channel velocities are significantly lower due to the influence of the pressure.

The following velocity contours within the reactor are presented for the discharging mode, analogous to those shown for the charging case. It is important to note that in this operating mode, the flow direction is reversed, moving from the bottom to the top of the (charged) reactor.

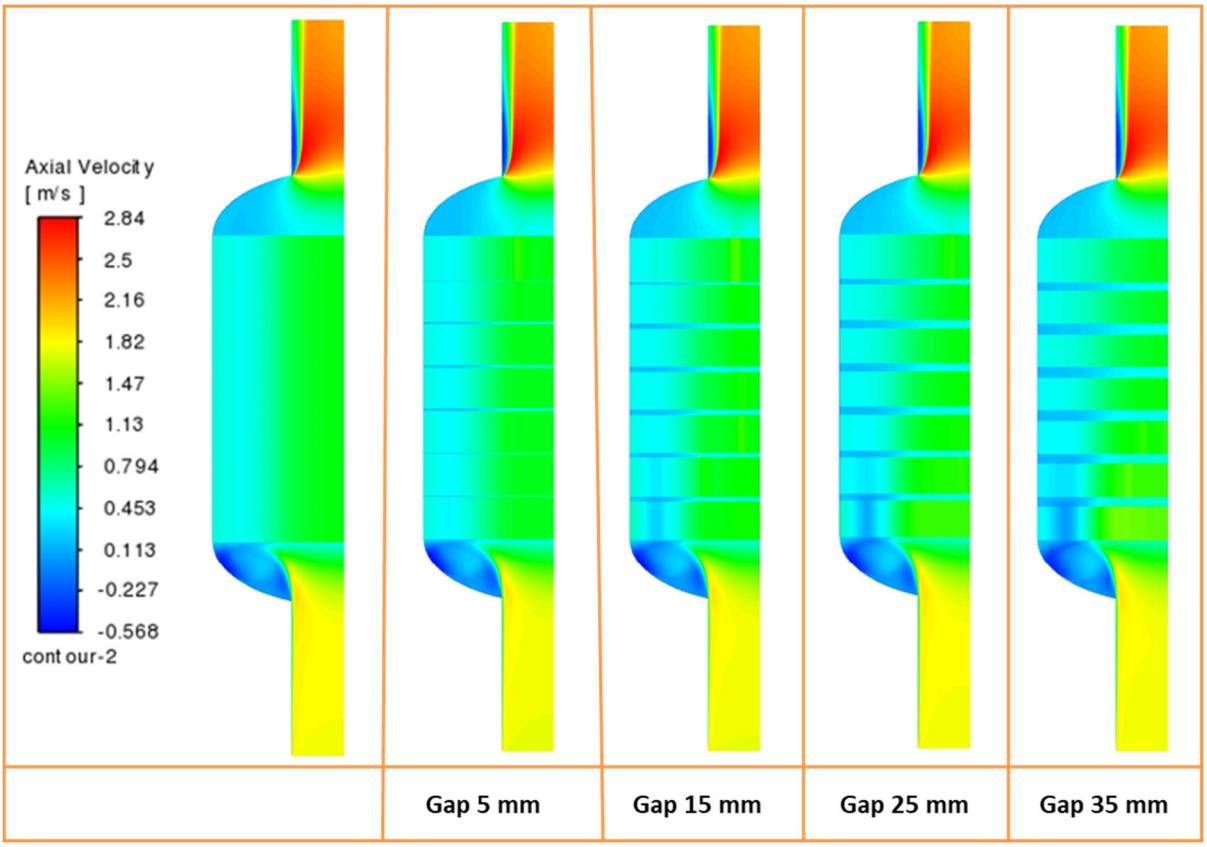

Figure 25: Velocity contours for discharging mode at different gap sizes.

Similarly to the charging case, the following graph presents the uniformity index for the discharging mode, providing a quantitative measure of flow distribution uniformity within the reactor under these operating conditions.

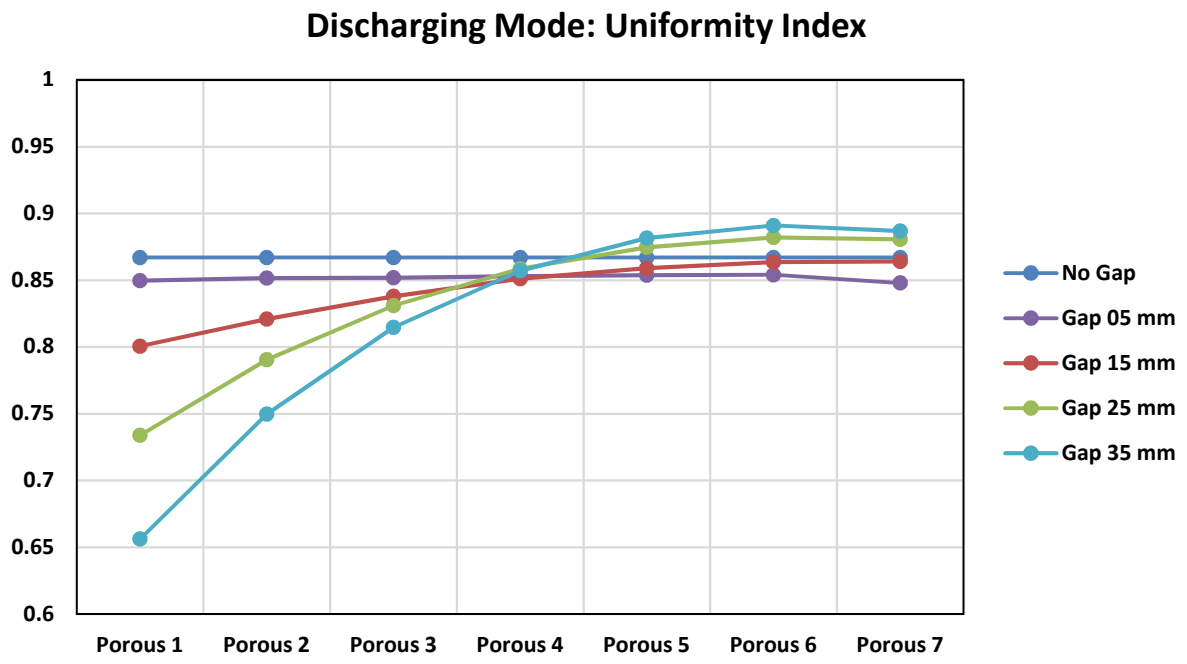

Figure 26: Uniformity index in each 7 honeycombs along the reactor for varying gap sizes in charging mode.

In this case, the uniformity index is slightly higher than in the charging mode, although the values remain generally low, indicating suboptimal flow uniformity. This is again attributed to the relatively low channel density in the honeycomb structures.

Nevertheless, the conclusions are consistent with those from the charging case: minimizing the gap between honeycomb sections is crucial to improving flow uniformity. As before, the final gap size will depend on the manufacturing tolerances and capabilities of the supplier.

4.6 Real Scale bed design

This section provides a synthesis of the design considerations and outcomes derived from prior analyses and the corresponding obtained results.

The **optimal matrix length** has been determined to be **1 meter**, primarily constrained by the **maximum allowable pressure drop** across the charged matrix.

Within this length, only approximately **67%** of the material reaches temperatures high enough to activate the **redox reactions** in the thermochemical medium and enable **chemical energy storage**.

The remaining portion of the matrix could theoretically be replaced with a **sensible heat storage material**. However, as observed with the sensible material developed in this project, reductions in **density** and **specific heat capacity** can adversely affect key performance indicators such as the **cycle duration** and the **average outlet temperature** toward the turbine.

As such, the final material configuration will be selected based on a comprehensive techno-economic analysis.

In terms of the **number of regenerative systems** required, this depends primarily on the **diameter of the bed**. During the design phase, simulations were conducted assuming the same chamber diameter as in the CAPTure project (0.83 m), and under this configuration, approximately **12 regenerative systems operating in parallel** would be needed to supply the required power for a **1.5 MWe turbine**.

However, it was found that increasing the **bed diameter** to, for instance**, 3 meters**, would allow for the use of a **single regenerative system** to achieve the same power output.

Once again, the final decision regarding the system configuration will be guided by a techno-economic evaluation, considering additional factors such as the cost of high-temperature and high-pressure vessels, as well as the valves required for chamber switching, which must withstand both high temperatures and significant pressure differentials.

Additionally, the impact of the **vertical spacing between successive rows of porous structures** was investigated to move toward a more realistic and manufacturable/practical design. The results indicate that a minimal vertical gap is optimal to achieve a uniformity level comparable to the ideal case (i.e., perfect stacking of porous elements to form continuous flow channels throughout the chamber length without obstructions).

5. Prototype Scale Dual-Bed Regenerative Matrix Design

This section presents the prototype-scale design of the regenerative bed, developed based on the previously established full-scale design. The prototype aims to enable testing under close-to-realistic solar irradiation conditions that will be carried out in next steps within the project.

Since the **total length** of the full-scale chamber (1 m) is a manageable dimension, the most straightforward approach for scaling is to use the same length for the prototype bed. Therefore, the plan is to construct a portion of the chamber while maintaining its original length.

Following this approach, regarding the **operating conditions**, the same temperature and pressure levels must be reproduced (see specifications section), and the same design flow rate to total flow area ratio resulting from the full-scale design should be maintained. The latter, based on the charging operation, was established as 0.6 kg/s over an area corresponding to a diameter of 0.83 m.

Regarding the **bed cross-section**, this parameter **can actually be adapted as long as the aforementioned flow rate to flow area ratio is maintained**. This ensures that the fluid conditions as it passes through the porous structures are accurately emulated.

The available unit structures, both thermochemical and sensible, have a cubic shape (150x150x150 mm). However, each matrix will be embedded within a pressure vessel, which has a circular cross-section. Therefore, it would be optimal for the matrix itself to have a circular cross-section as well, in order to minimize edge gaps and facilitate internal insulation. To achieve this, the same technique currently used for manufacturing segmented diesel particulate filters (LANDSON) will be employed, where the circular section is assembled from multiple square-cross-section units, some of which are truncated at the periphery as in Figure 27a, or, alternatively, from two shapes of extruded circular segments as in Figure 27b.

Regarding the **composition of the bed**, the direct conclusion from the design process is to use a minimum of 67% thermochemical material in the matrix (the section near the air inlet during charging), employing only sensible heat material for the remaining length (the section near the air outlet during charging). However, given the manageable length of the prototype and its goal to maximize experimental capability, the ideal design for the test rig would allow easy replacement of structures. This would enable experimental comparison, for example, of the suitability of maintaining the entire matrix with thermochemical material versus the initial premise of substituting part of the length with only sensible heat material. Furthermore, as the project continues to evolve in both material development and the production of corresponding structures (different porosities, etc.), it makes sense to incorporate this versatility to allow testing of various future compositions, porosities, and other parameters.

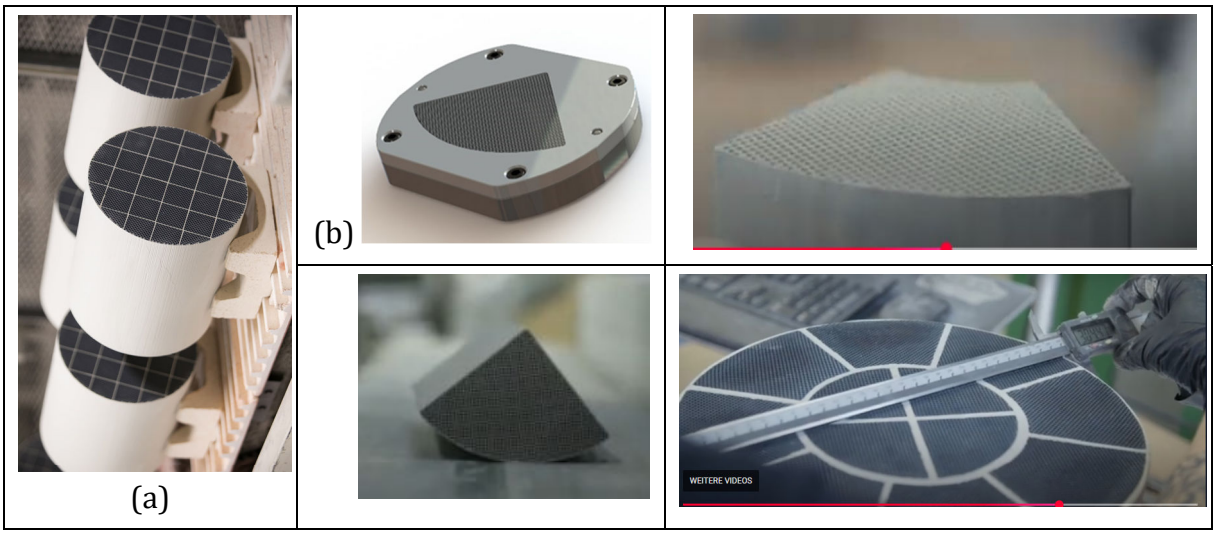

Figure 27: (a) Circular cross section bed structures assembled from unitary structures of tetragonal cross-section (https://www.ibiden.com) (b) extrusion die and typical segments extruded in LANDSON for the assembly of cylindrical honeycomb structures (https://www.landson.dk/dpfs)

6. Sensitivity Analysis on identified potentially important parameters

In addition to the core design activities, a sensitivity analysis was carried out to explore the potential impact of modifying certain parameters currently imposed as fixed design constraints. While these constraints were initially defined based on upstream or external system requirements, their relaxation could open opportunities for performance enhancement in future developments.

Specifically, two parameters were examined: the cell density of the porous structures—keeping overall porosity constant—and the maximum allowable outlet temperature during the charging phase, which is limited by the specifications of the low-temperature storage system.

By analysing the influence of these parameters on the system's thermal behaviour and efficiency, this study provides valuable insights into design flexibility and identifies potential levers for future optimization. These results do not affect the current design but serve to inform future iterations and guide experimental planning.

6.1 CPSI parameter

This parameter represents the number of channels in the porous medium per unit area (cell density). Within a relatively small increase in the cpsi parameter, it is possible to maintain bed porosity fairly constant or limit its decrease. This can be controlled by adjusting the ratio between cell (channel) size and wall thickness—an analysis that will

be carried out in WP3, informed by this sensitivity study. For the purposes of the current analysis, it is assumed that bed porosity remains constant for the specific cpsi change considered. WP3 will evaluate the validity and implications of this assumption, including potential effects on manufacturability, and will revise it if necessary. This assumption is crucial because the decision to analyze cpsi instead of porosity stems from the fact that increasing porosity—presumably making the structure more porous—would reduce the solid mass and, therefore, the thermal storage capacity. Thus, varying the CPSI (cells per square inch) without changing porosity may offer potential advantages.

The influence of this parameter is evaluated from two perspectives: its impact on the overall performance of the system and on the level of flow distribution homogeneity within the matrix.

Regarding its impact on flow distribution, the flow is not uniform when passing through the reactor filled with the porous structures. Therefore, two new CFD models have been developed—one for charging and another for discharging—in which the reactor is filled with a porous structure with higher CPSI: 147cpsi (HN2) instead of 59cpsi of the original structures (HN1). These models are constructed exclusively for the ideal case without any gap. The objective is to confirm that the observed lack of uniformity is due to the low number of channels per square inch, given that the new analysed structure has 2.5 times more channels per square inch than the original one.

Figure 28 shows the velocity contours inside the reactor during both charging and discharging, varying the number of cells per square inch. The velocity contours clearly show that using the HN2 structures significantly improves the flow distribution compared to HN1. This improvement is also quantitatively confirmed by the uniformity index graph presented earlier.

Comparing the values, the uniformity index for HN2 is nearly 0.95 (Figure 29), which is approximately 0.1 higher than that of HN1. This improvement aligns well with the better results previously obtained in the CAPTURE project.

Regarding the **impact in the global performance**, the behaviour of the system has been simulated comparing 1m length beds made up of thermochemical material of 30% porosity, and three different values of CPSI: 59 (REF), 105 (Case 2), and 236 (Case 1). Figure 30 shows the resulting thermocline profile at the end of the charging process.

So, the higher the number of channels the higher the stored energy and thus longer cycles and higher efficacy.

Based on these results, it is recommended to manufacture honeycombs with a higher number of channels per square inch to enhance flow uniformity through the bed and increase the storage capacity and the system performance.

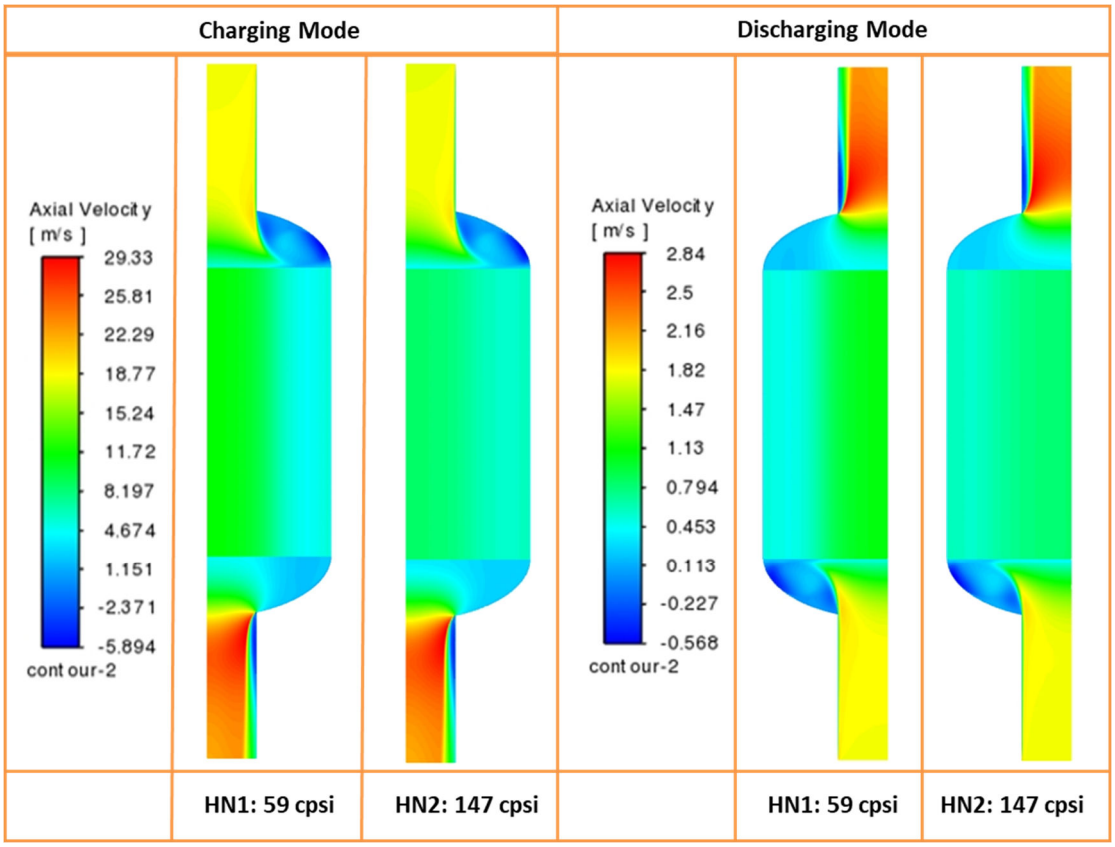

Figure 28: Velocity contours for HN1 and HN2 structures during charging and discharging.

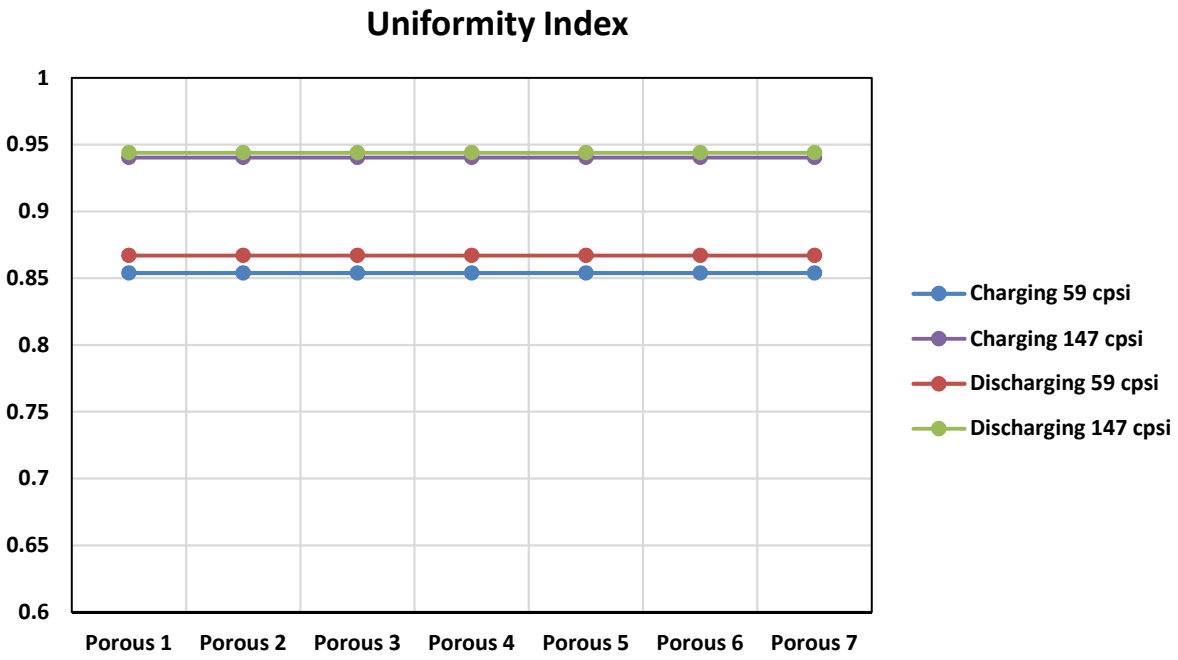

Figure 29: Uniformity index in each 7 honeycombs along the reactor for HN1 and HN2

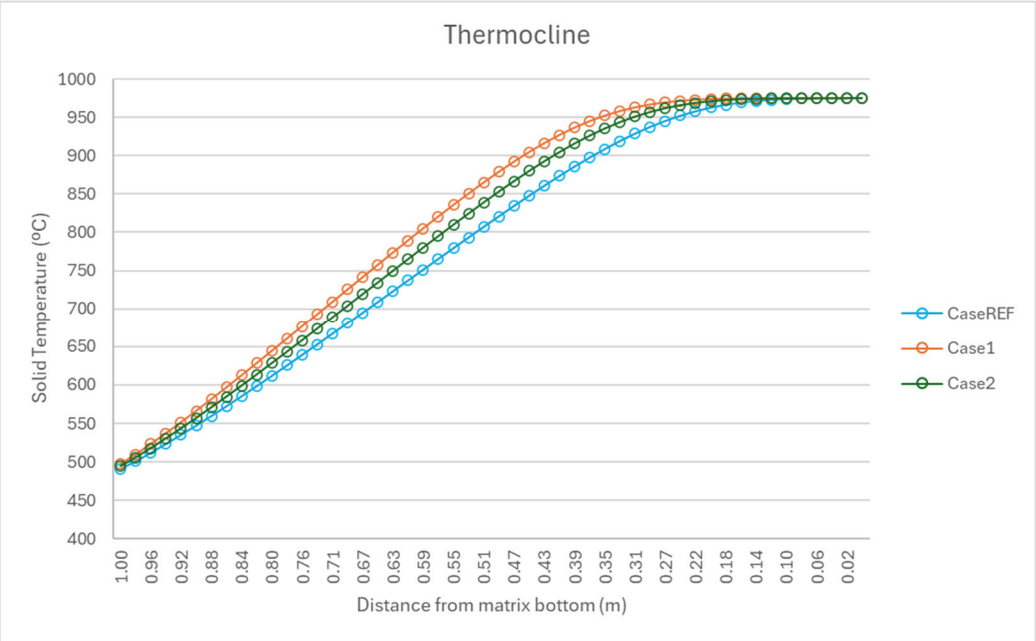

Figure 30: Thermocline profile at the end of charging process for different cpsi parameters of the porous structures.

6.2 Air outlet temperature in charging process

Currently, the design imposes a constraint on the maximum air temperature at the outlet of the matrix during the charging process. This temperature limit is set by the design of the thermal storage system, which consists of a high-temperature storage unit and a low-temperature one—the latter being the element that determines the current temperature cap.

However, this constraint could be revised if doing so leads to a more favourable overall plant performance. In such a case, the maximum temperature could instead be limited by other system components, such as the maximum allowable temperature for specific valves in the regenerative system. In this scenario, new target temperatures in the range of approximately 700 °C could be considered.

From the perspective of the regenerative system and matrix design, increasing this outlet temperature would enhance the amount of energy stored during charging and lead to a flatter thermocline within the charging bed.

The following graph shows the air temperature at the outlet of the regenerative unit in discharge for the 1-meter-long regenerative bed, in blue for the case of the limit temperature of 500ºC and in red for the case of the limit temperature of 600ºC. When the maximum temperature is increased to 600 °C, the cycle time extends to 24.5 minutes, compared to 14 minutes at 500 °C. This allows the bed to store more energy but also results in a lower minimum outlet air temperature during the discharge phase (red line)—dropping to 712.5 °C, versus 846 °C at the lower temperature setting, which leads to a lower efficiency of the regenerator.

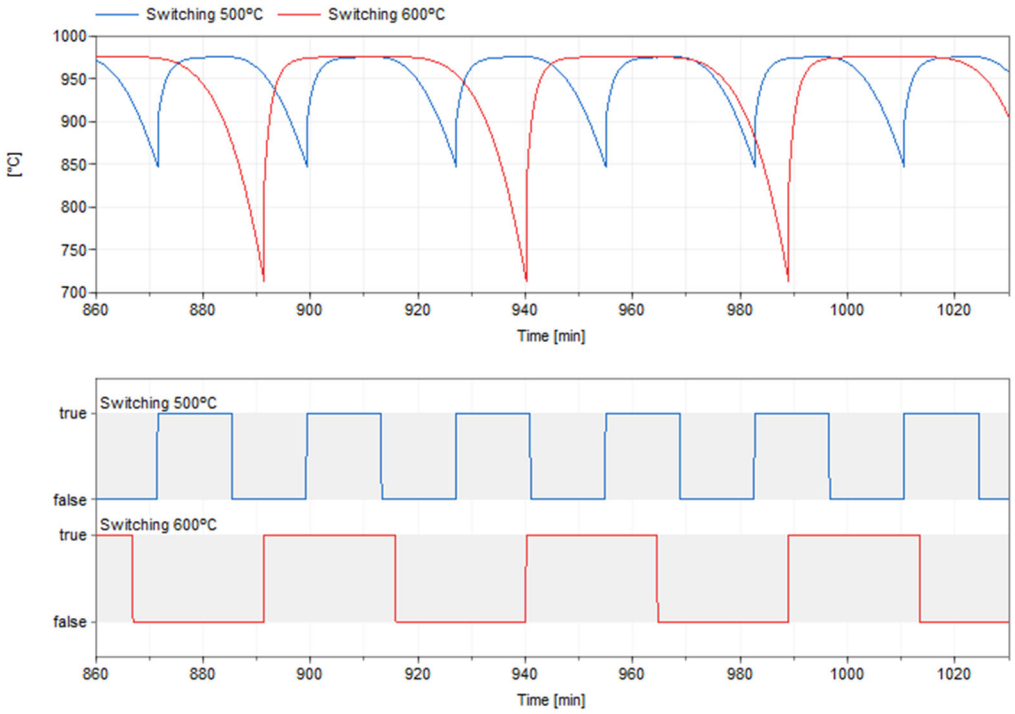

Figure 31: Simulation results in TC+OS1 when switching limit is 500ºC vs when is 600ºC

Increasing the maximum operating temperature allows the regenerative bed to store a greater amount of thermal energy during the charging phase. As expected, reaching this higher temperature takes more time. Since the system operates in a synchronized charge/discharge cycle, the discharge phase is also extended. This results in longer switching periods, and consequently, a more noticeable drop in the outlet air temperature over time during the discharge.

As commented at the beginning of the section, this temperature limit could be further increased, actually only conditioned by the maximum allowed temperature at the valves (around 700ºC). However, tests have shown that raising this value to 700 °C also leads to lower minimum outlet air temperatures during the discharging phase—below the value corresponding to the 25% load of the turbine, potentially complicating the control strategy of the regenerative system (to be developed further in the project) during switching phases, as observed in the CAPTure project.

This lowering in the minimum outlet temperature towards the turbine could be improved by selecting a different value for the charging mass flow rate (from receiver/storage) with respect to the discharging mass flow rate (from turbine). However this would need further analysis since it would involve important modifications to the system (modifying the length of the bed, etc.) and the corresponding technoeconomic analysis.

7. Conclusions

This document has detailed the design process for the regenerative beds at both full-scale and prototype-scale levels, highlighting the key considerations, design choices, and results obtained.

For the **full-scale design**, the optimal matrix length was established at 1 meter, primarily limited by the maximum allowable pressure drop during operation. Within this length, approximately 67% of the thermochemical material reaches temperatures sufficient to activate redox reactions and store chemical energy, while the remaining length may be substituted with sensible heat material. However, this substitution affects important parameters such as cycle duration and average outlet temperature, making the final material selection dependent on a thorough techno-economic assessment. Additionally, the number of regenerative systems needed is highly influenced by the chamber diameter: a diameter of 0.83 m would require about twelve parallel systems for a 1.5 MWe turbine, whereas increasing the diameter to 3 m could reduce this to a single system. This decision will ultimately be guided by techno-economic factors, including vessel and valve costs and operating conditions. The investigation of vertical spacing between porous structure layers further indicated that minimal gaps yield flow uniformity close to theoretical ideals, enhancing design realism and manufacturability.

Moreover, the **influence of certain parameters**—currently defined as design requirements—has also been explored with a view to potential future design flexibility. Specifically, the number of channels within the porous structures (while maintaining porosity) and the maximum allowable outlet temperature during charging (a constraint inherited from the low-temperature storage system) have been examined. Adjustments to these parameters could lead to improved system performance, and thus they are identified as promising levers for future optimization beyond the present design constraints.

The **prototype-scale design** builds directly upon the full-scale design, maintaining the 1-meter length to facilitate manageable testing under near-real solar irradiation conditions. The prototype replicates the full-scale operating conditions—temperature, pressure, and flow rate to flow area ratio—to accurately emulate fluid dynamics within the porous bed. While the cross-sectional area can be adjusted, the design must accommodate cylindrical pressure vessels, requiring porous structure arrangements that maximize area coverage and minimize lateral gaps. Two structural approaches were considered: using multiple cubic units to fill the cross-section, or a single cylindrical structure that better fits the vessel geometry and simplifies insulation and flow distribution. The latter offers advantages in flow uniformity and vessel integration but limits the test section size and experimental exploration of porosity variations.

Regarding bed composition, the design calls for at least 67% thermochemical material near the air inlet during charging, with the remainder potentially replaced by sensible heat material near the outlet. Given the prototype's experimental role, flexibility

to interchange structures is critical to compare different material configurations and to explore evolving materials and porosities as the project progresses.

In summary, the combined design efforts have established a robust foundation for both practical full-scale deployment and flexible prototyping. The full-scale design balances thermal performance with system complexity and cost, while the prototype facilitates experimental validation and material testing under realistic conditions. Future work will focus on techno-economic optimization and experimental campaigns to refine and validate these designs.

8. References

[1] S. López, J. Febres, I. Mesonero, "System 1-D dynamic model report and open-source model library",Competitive SolAr Power Towers – CAPTure project results (CORDIS, 2016).

[2] I. Mesonero, J. Febres, S. López, "Modeling and simulation of fixed bed regenerators for a multi-tower decoupled advanced solar combined cycle", Proceedings of the 12th International Modelica Conference (Prague, CzechRepublic, 2017) pp 847-855

[3] I. Mesonero, S. López, I. Del Hoyo, S. Kunze, S. Herrero, "Regenerator-type connection between a volumetric receiver and a high efficiency turbine. Design and optimization. Poster at SolarPACES Conference 2018.

[4] S. Herrero, S. López, J. McGuire, "Matrix and Control Design of Fixed Bed Regenerators for a Multi-tower Decoupled Advanced Solar Combined Cycle", SolarPACES 2020 AIP Conference Proceedings 2445, 060003 (2022)